Charles University in Prague

Faculty of Mathematics and Physics

DOCTORAL THESIS

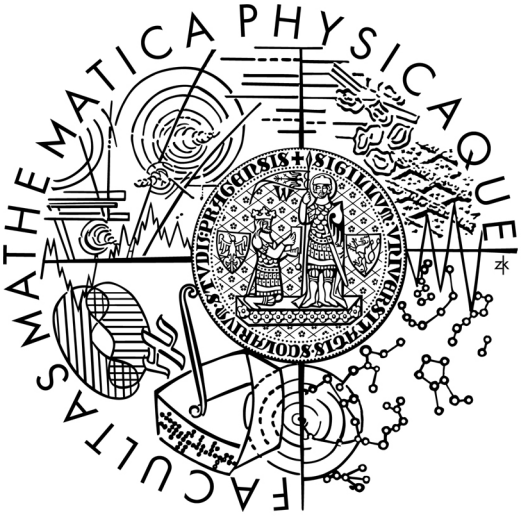

Shirly Josefina Espinoza Herrera

Function of Magnesium Ions in the Formation of Biologically-Active Nucleic Acids Structures

Institute of Physics of Charles University

Supervisor: prof. RNDr. Josef Štěpánek, CSc.

Study program: Physics
Biophysics, chemical and macromolecular physics

Acknowledgement

I specially thank to my supervisor Prof. RNDr. Josef Štěpánek, CSc. for his help, his advices, and his patience. I also thank to all the staff of the Institute of Physics that in different ways helped me during my studies.

I declare that I have written this doctoral thesis by myself using only the quoted sources. I agree with lending this doctoral thesis.

Prague, December 10, 2010

Shirly Josefina Espinoza Herrera

ABSTRAKT

Byla studována interakce hořečnatých iontů, jež jsou divalentními ionty s nejvyšší koncentrací v živých buňkách, s klíčovými biomolekulami nukleových kyselin, s cílem zjistit strukturní detaily mechanismu této interakce a účinek hořečnatých iontů na strukturu a strukturní přechody u nukleových kyselin. Jako hlavní metoda byla vybraná Ramanova spektroskopie; kromě toho byla provedena I některá doplňková měření UV absorpce. Základní analýzy sérií spekter získaných v závislosti na teplotě a případně při různých koncentracích hořečnatých iontů byly prováděny pomocí faktorové analýzy. Kde to bylo možné, sloužily výstupy faktorové analýzy při fitování odpovídajících termodynamických vztahů.

Ke studiu byly použité různé molekulární modely nukleových kyselin, konkrétně systém komplementárních RNA homopolynukleotidů polyA a polyU, DNA homopolynucleotidů polydA a polydT, a RNA 14-merní oligonukleotid představující vrcholovou vlásenku segmentu TAR genomické RNA viru HIV-1.

Potvrdili jsme pomocí Ramanovy spektroskopie, že ionty hořčíku přidané do roztoku polyA-polyU duplexů způsobí jejich částečnou disociaci a vytváření triplexů. Získali jsme ramanovskou charakteristiku specifického vazebného místa lokalizovaného ve žlábku mezi polyA řetězcem a hoogsteenovským uridylovým vláknem.

Tato disertační práce také poprvé prezentuje výsledky studia vlivu hořečnatých iontů na jemné “premelting” přechody. Na dvou modelových systémech, polydA-polydT duplexu a vrcholové TAR vlásence, bylo ukázáno, že hořečnaté ionty ovlivňují tyto přechody v měřitelné míře, ale zcela rozdílně. V případě duplexu polydA-polydT je účinek hořčíku mnohem silnější a týká se především stabilizace nízkoteplotní konformace. V případě vrcholové vlásenky TASR je hlavním výsledkem působení hořečnatých iontů podpora strukturního uspořádání bází nukleových kyselin ve smyčce vlásenky, které se objevuje při teplotách nad “premelting” přechodem.

ABSTRACT

Interaction of magnesium ions, the divalent ions with the highest concentration inside living cells, with the key biomolecules of nucleic acids was studied with aim to find out structural details of the interaction mechanism and effect of the magnesium ions presence on the nucleic-acid structure and structural transitions. Raman spectroscopy was chosen as the main experimental method, some complementary measurements of UV absorption spectra were also performed. Basic analyses of the spectral series obtained as a function of temperature and/or for various concentrations of Mg^{2+} ions were done by means of factor analysis. Where possible the factor analysis outputs were used for fits of appropriate thermodynamic equations.

For the studies, various nucleic-acid molecular models were employed, in particular complementary RNA homopolynucleotides polyA and polyU, DNA homopolynucleotides polydA and polydT and RNA 14-mer oligonucleotide representing the apical hairpin of the TAR segment of HIV-1 genomic RNA.

We have confirmed via Raman spectroscopy that magnesium ions added to a solution of polyA-polyU duplexes force some of them to dissociate and to form triplex structures, and obtained Raman signature of the specific binding site, being in the major-major groove between the adenyl and the Hoogsteen uridyl chain.

The thesis also presents the first study of magnesium ions effect on subtle premelting transitions. It was demonstrated on two model systems, poly(dA)-poly(dT) duplex and apical TAR hairpin, that magnesium ions influence them measurably, but in quite different ways. In the case of poly(dA)-poly(dT) duplex, magnesium effect is much stronger and concerns mainly the stabilization of the low temperature conformation. In the case of the apical TAR hairpin, the main effect of magnesium ions is the support of the structural changes in favor of the arrangement of the nucleobases in the hairpin loop reached at the temperature above the premelting.

CONTENT

LIST OF TABLES

LIST OF FIGURES

1. INTRODUCTION

Nucleic acids are negatively charged polyions that need positive ions to form different structural conformations and carry out their function. This work presents the results of the studies of the influence of magnesium ions on different types of nucleic acids structures.

Homopolynucleotides, sequences of nucleotides with only one kind of base, are present in different biological systems and they are extensively used like model systems for the studies on nucleic acid structures of several strands. In this work, complementary RNA homopolynucleotides, polyA and polyU, and complementary DNA homopolynucleotides, polydA and polydT, were chosen as models for the study of the effect of magnesium ions on double and triple strands of polynucleotides. RNA oligonucleotide, the 14-mer apical hairpin of the TAR segment of HIV-1, was also studied. More details about the studied nucleic acid systems will be explain in next section, which begin with a review of the literature related with nucleic acid structures and their interaction with ions.

This study on the effects of magnesium ions on nucleic acids was done by Raman spectroscopy and UV absorption spectroscopy. These methods are described in the section called ‘experimental’, where the protocols for the preparation of the samples and the equations used for the treatment of the data obtained in the experiments are also explained. The results are presented and discussed in the forth section. The conclusions are summarized at the end of this work.

2. NUCLEIC ACIDS AND DIVALENT IONS

Nucleic acids (NA) are macromolecules that store all information required to make and maintain a living organism. Two basic groups of nucleic acids can be distinguished, i.e. deoxyribonucleic acid (DNA) and ribonucleic acid (RNA). The DNA stores the genetic information in all living organisms with exception of some viruses (which instead use RNA as their genetic material); RNA enables the translation of the genetic information into proteins.

The nucleic acids are polymeric molecules whose monomers are called nucleotides. The nucleotides are formed by a phosphate group, a sugar – ribose (RNA) or 2'-deoxyribose (DNA) – attached to the phosphate by an ester bond, and a heterocyclic base connected to the sugar via a β C'1-N glycosyl linkage. The major bases in DNA are adenine (A), guanine (G), cytosine (C), and thymine (T). In RNA the major bases are the same except that the base uracil (U) is used in place of thymine (T).

Adjacent nucleotides are linked together through a phospodiester bond in which the phosphate group connects the 5’-end of one sugar to the 3’-end of the next. The polymerization of nucleotides generates long, single-stranded polyanionic chains. The nucleobase sequence (read in a 5’- to 3’ direction) constitutes the primary structure of nucleic acid (Figure 2.1)

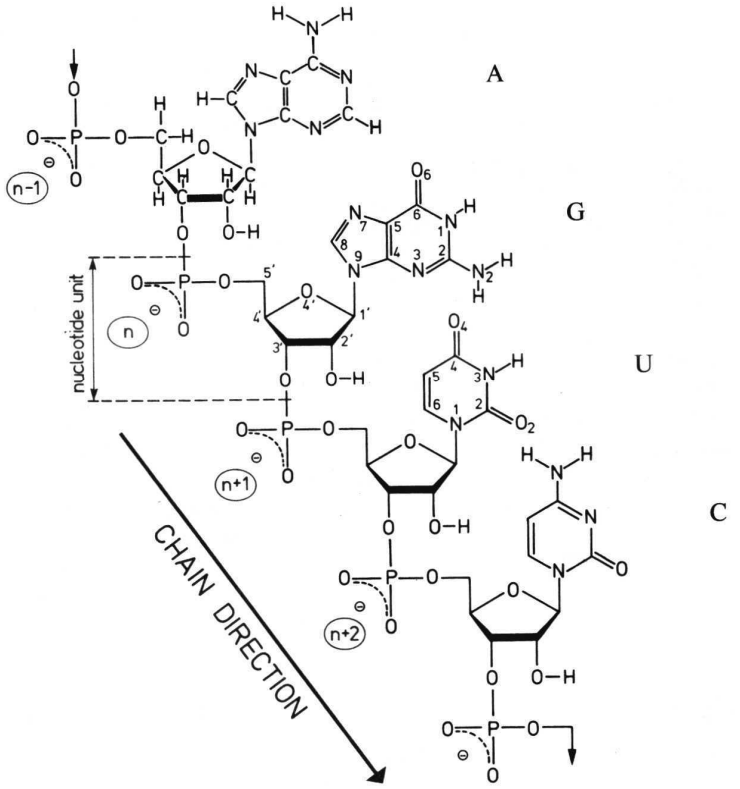

FIGURE 2.1. Schematic representation of an RNA fragment containing the four major RNA nucleobases. The standard numbering scheme of the sugar, purine and pyrimidine atoms is shown [1].

2.1 POLYMORPHISM OF NUCLEIC ACIDS

In organism, NA are packaged and organized in higher-ordered forms. The DNA is dominantly found as duplex structures. Inter-strand hydrogen bonds between bases hold together the two strands of the duplex. In the most common “base-pairing”, proposed in the beginning of the 1950's by James Watson and Francis Crick (Figure 2.2), the bases of adenine and thymine specifically hydrogen-bond each other (A-T), the same as the base pair guanine and cytosine (G-C). The distance between the two glycosylic bonds for both the A-T and the C-G basepairs is of 10.60 ± 0.15 Å with an angle between the C-1'…C-1' line and the glycosyl bond of 68 ± 2º. The stability of the double-helical arrangement is further supported by π–π interactions between the stacked hydrophobic aromatic rings of adjacent bases on the polynucleotide chains.

Each strand of the double helix can serve as a matrix for DNA replication. It enables storing, expression and transmission of the genetic information, which are the main purposes of nucleic acids.

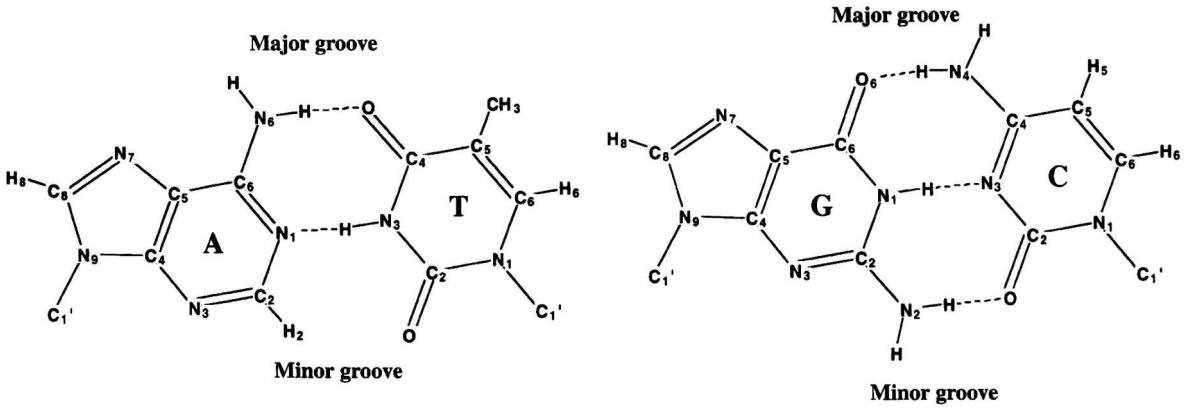

FIGURE 2.2. Schematic description of Watson–Crick base pairs. Hydrogen bonds are indicated by dotted lines [2].

Unlike DNA, in living organisms RNA is rarely composed of two strands base paired with each other. Instead, RNA exists as a single-stranded entity, though extensive regions of many RNAs may form double helices within themselves by the base pairing rules. Ribonucleic acids can fold into a variety of complex structures involved in many of the biochemical reactions needed for protein biosynthesis, chromosome-end replication, gene expression, and protein transport.

There is a variety of other, non-canonical base-pairings found mainly in RNA, the most important are Hoogsteen pairs and Crick ‘wobble’ pairs. Hoogsteen pairs have an 80º angle between the glycosylic bonds and an 8.6 Å separation of the carbons. Hoogsteen base pairing can be found, for example, in the U:A*U or C:G*C+ triple helices (see Figure 2.6).

Duplexes

Duplex nucleic acids are able to adopt a variety of different conformations influenced by the primary structure (base sequence) and environmental factors like temperature, concentration of monovalent and divalent ions, etc. The conformational form of DNA most commonly encountered under physiological

conditions (relatively high hydration, low ionic strength) is known as B-DNA and it was first described by Watson and Crick in 1953 [3]. The right handed B-DNA helix (Figure 2.3 and Table 2.1) has a diameter of approximately 20Å, 10.5 base pairs per turn and a 3.4Å step between base pairs that are nearly perpendicular to the helical axis. The sugars have the C2'-endo pucker, this ‘puckering' is assigned according the major displacement of carbons-2' and -3' from the median plane of C1'-O4'-C4'. If the endo displacement of C-2' is greater than the exo displacement of C-3' the conformation is called C2'-endo [4].

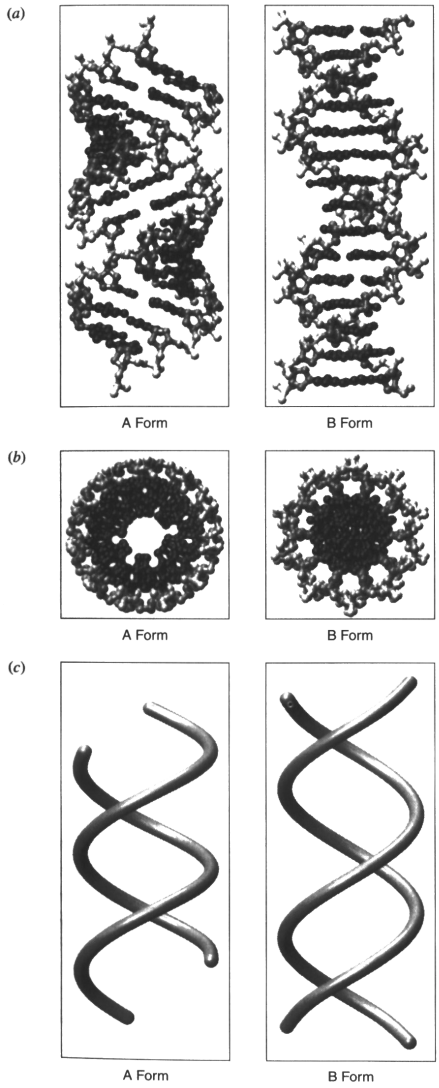

FIGURE 2.3. A and B Basic canonical forms of nucleic acid duplexes. Each containing 20 base-pairs. (a) Ball-and-stick side views, (b) ball-and-stick end views, (c) cylindrical ribbon representation (Adapted from [1]).

The outer lining of the molecule presents two grooves that run the length of the duplex, as the strands are not directly opposite each other, the grooves are unequally sized. There exists a wide (11.6Å) major groove and a narrow (6.0 Å) minor groove, with both grooves being of a similar depth (ca. 8 Å). However, these dimensions are sensitive to the base sequence; for example, AT-rich sequences are known to adopt a narrower and more flexible minor groove than GC-rich regions. As a rule of thumb, the minor groove is at the O2 (pyrimidine) or N3 (purine) side of the base-pair and the major groove is on the opposite side.

TABLE 2.1. Selected parameters of basic canonical forms of nucleic acid duplexes [5,6].

Attribute	B double helix	A-double helix
Helical sense	right-handed	right-handed
Bp per repeating unit	1	1
Base pair per turn	10.5	11
Rotation per bp	36°	33°
Rotation per bp	3.4 Å	2.6 Å
Major groove width	Wide. 11.6 Å	Narrow. 2.2 Å
Major groove depth	Deep. 8.5 Å	Deep. 13.0 Å
Minor groove width	Narrow. 6.0 Å	Wide. 11.1 Å
Minor groove depth	Deep. 8.2 Å	Shallow. 2.6 Å
Sugar pucker	C2'-endo	C3'-endo
Glycosyl angle	*anti*	*anti*

When the concentration of cations is high, the DNA assumes a wider, more compact structure (11 bp per helical turn) know as an A-form (Figure 2.3 and Table 1.1.). The bases are displaced toward the periphery of the double helix resulting in an essentially empty core. The major groove of A-DNA is very deep and narrow; in opposition, the minor groove is wide and shallow. Duplex RNA commonly adopt this A-type conformation – a result of the 2'-hydroxyl group of ribose forcing the

RNA sugar into a C3'- endo (C2'-exo) conformation rather than the C2'- endo arrangement characteristic of B-DNA.

It is understandable that NA can form a variety of other polymorphic structures of biological importance, considering, for example, the 3 billion base pairs in the human genome, which means a 2 m long molecule packaged in a cellular nucleus. These other polymorphic forms are assigned to a one-letter code (following the nomenclature adopted in the original studies of NA structures, of assigning the letters A, B, etc.), currently there are DNA structures associated with 21 of the 26 letters of the English alphabet (only the letters F, Q, U, V and Y have not been used yet). [7]

The ability of NA molecules to assume various forms has made the NA research evolved towards nonbiological fields like the application in nanotechnology: nanomachines which direct the assembly of highly structured materials with specific nanoscale features, as well as in DNA computation to process complex information [8].

Hairpin loops

Hairpin loops (also called stem-loops) occur when a polynucleotide chain possessing self-complementary bases loops back on itself to form a duplex stem terminating in a loop of unpaired bases followed by a stem with duplex structure (Figure 2.4). In DNA the stem usually assumes a B-type conformation, while in RNA it is typically of the A-form. In several studies, the stability of hairpin structures has been found to be governed by the length and sequence of the loop rather than the sequence of the stem [9]. DNA loops are typically associated with mutagenic events and tend to be temporary.

Hairpin loops are much more frequent in RNA providing stabilizing contacts and nucleation sites for RNA folding, as well as protein recognition sites. The 16S rRNA has 70% of its length folded into 31 hairpin-loop structures. The tRNA structure comprises three stem-loop structures playing a significant role in its tertiary

structure and function. The TAR and RRE HIV mRNAs also have stable hairpin loop structures involved in binding-site recognition by the Tat and Rev proteins, respectively. Stem-loops structures also appear in the ends regions of mRNAs where they are supposed to modulate its longevity.

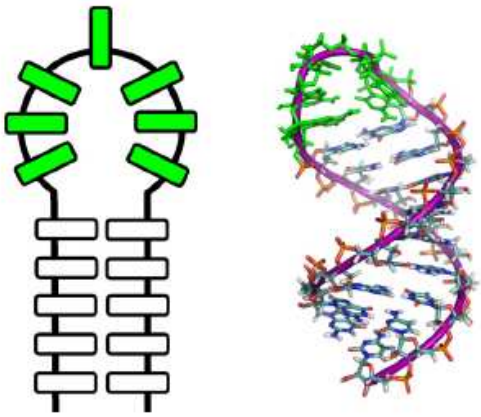

FIGURE 2.4. Hairpin loop. Schematic representation of a hairpin loop and the NMR structure of a conserved rRNA 5-base loop (PDB identifier 15ki) Unpaired bases are depicted in green [5].

Multiplexes

Certain nucleic acid sequences are able to form complexes of more than two strands (Figure 2.5). Two types of triplex have been characterized, depending on the orientation and base composition of the third strand. Pyrimidine-rich oligonucleotides, (or Y.R:Y) motif, bind parallel to the duplex purine strand, that in the case of DNA would generate T•AT and C+•GC triplets and in the case of RNA, U•A*U triplexes. These Y.R:Y motifs consist of a homopurine-homopyrimidine tract of a normal Watson-Crick duplex that accept a third pyrimidine strand into its major groove via the Hoogsteen base-pairing scheme (Figure 2.6). The formation of C+•GC parallel triplexes is limited by the requirement for low pH for the protonation of the third-strand cytosines.

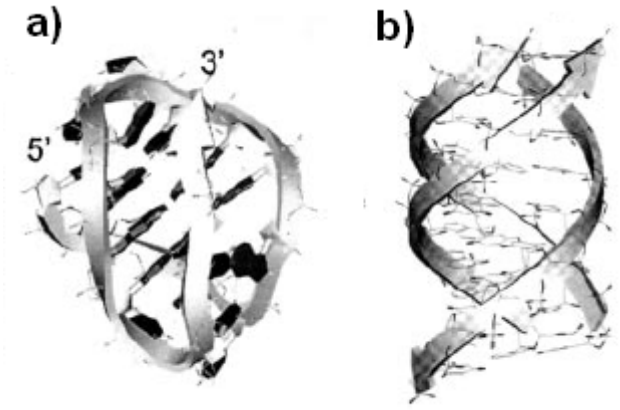

FIGURE 2.5. Multiplexes. Multistranded NA structures. a) quadruplex, b) triplex. [10]

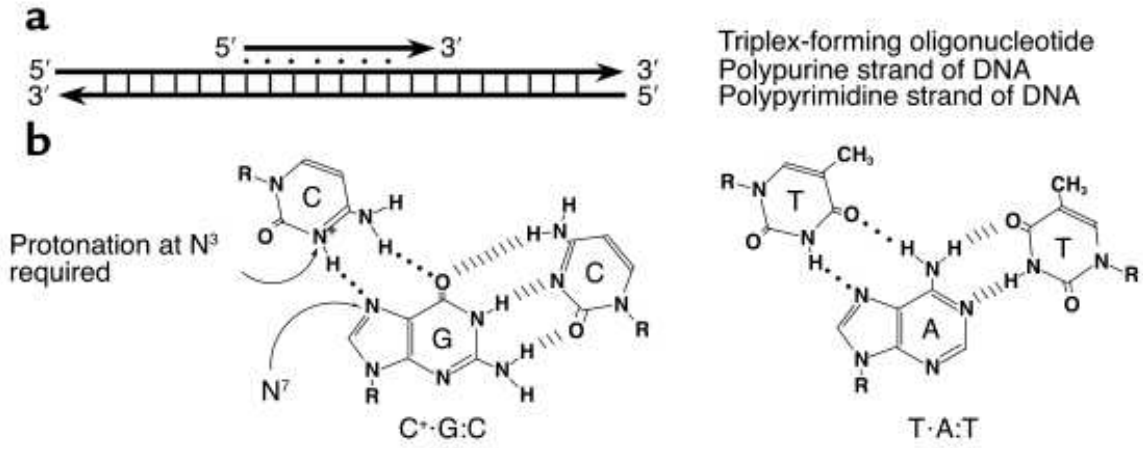

FIGURE 2.6. Diagram of a pyrimidine motif for triple helix formation. (a) Orientation of the third strand in the pyrimidine triple-helix motif. (b) Base triplets formed in the pyrimidine motif and illustration of the Hoogsteen hydrogen bonds that stabilize triple-helix formation [11].

The addition of a third strand to form the triplex divides the major groove of the double helix into a major-minor groove and a major-major groove. The three grooves that are named according to the bonding scheme between the strands that define each groove; i.e., there is a Watson-Crick groove (the minor groove of the double helix), the groove between the purine strand and second pyrimidine strand is called the Crick-Hoogsteen groove, and the third groove (between the two pyrimidine strands) is called the Watson-Hoogsteen groove.

The third strand can also be a purine strand. The purine-rich oligonucleotide then bind as the third strand in an antiparallel orientation (Figure 2.7), forming R.R:Y motif like A•AT or G•GC. This way of binding requires reverse Hoogsteen base pairing schemes [13]. And it is also possible to have this kind of scheme in T•AT triplexes.

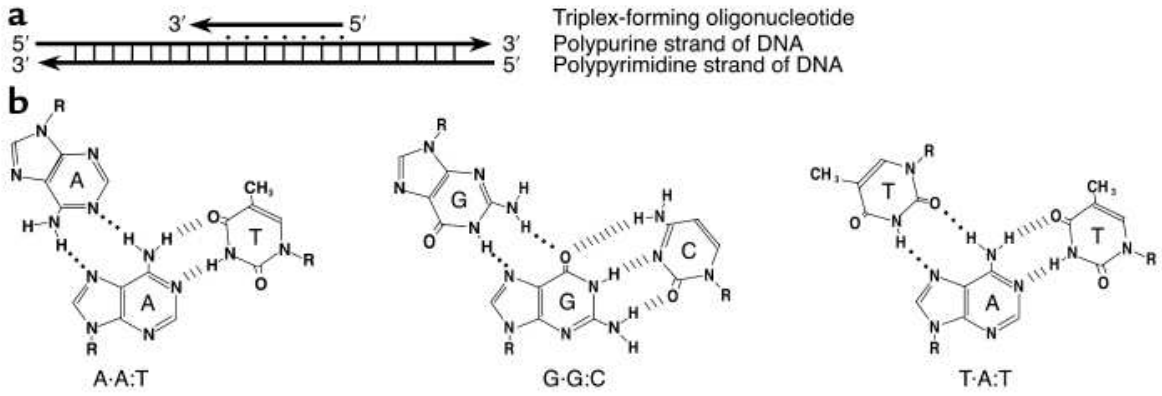

FIGURE 2.7. Diagram of the purine motif for triple helix formation. (a) Orientation of the third strand in the purine triple-helix motif. (b) Base triplets formed in the purine motif and illustration of the reverse Hoogsteen hydrogen bonds that stabilize triple-helix formation [11].

An in vivo role of triple helices has not been established yet; however, synthetic triplex-forming strands show promising application as diagnostic and therapeutic agents, the binding of the third strand may be used for modulating gene expression or as a sequence-specific cleavage agent. Double-stranded DNA sequences can be specifically recognized by synthetic oligonucleotides. The formation of intermolecular triple helices (TFO, triplex-forming oligonucleotides strategy, or “antigene strategy”) is being studied as a possibility to modulate biological processes such as transcription, DNA replication, DNA repair and recombination [11]. Similarly, sequence-specific mRNA recognition by specially designed oligonucleotides (following duplex formation) could make possible the use of duplexes to cure diseases caused by RNA-containing viruses (including AIDS) this pharmacologically important field of investigation is called “antisense” strategy” [12].

Other significant multistranded nucleic acid configuration is the quadruplex. They are usually associated with guanine-rich sequences. The *in vivo* role of quadruplex DNA is connected to its formation in telomeres, where quadruplexes can impede telomerase activity and then, quadruplex stabilizing agents are seen as a good alternative for fighting against cancer.

Other conformations

There exist other varieties of conformations adopted by nucleic acids that would not be treated in this work.

Bulges: Bulges are deviations from the canonical duplex of nucleic. They occur when one strand of the hydrogen-bonded duplex possesses one or more nucleotides with no counterpart on the opposing strand (Figure 2.8). As it occurs with hairpin loops, in DNA, bulges are not common but they are present in RNA secondary structures as potential protein recognition sites.

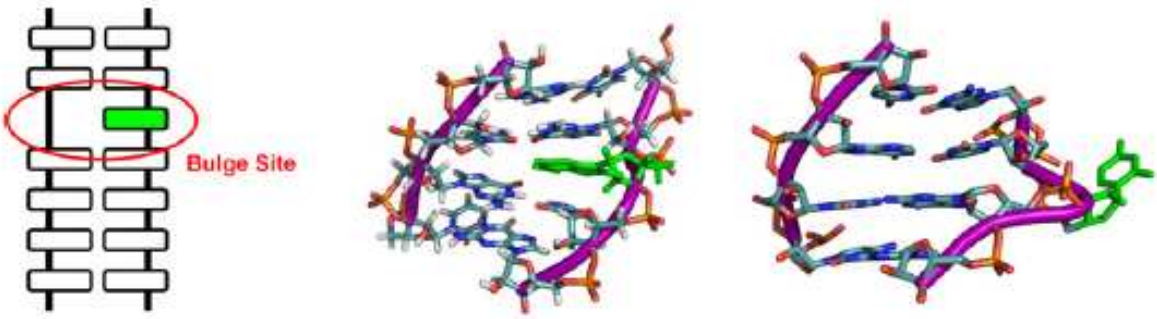

FIGURE 2.8. Representation of a single-base bulge site. The unpaired base depicted in green. Left-to-right: schematic of a single-base bulge; render of PDB NMR structure 1rht, a bacterial coat protein RNA binding site, featuring an intrahelical unpaired adenine; and a render of PDB crystal structure 1dqh, a section of 5S rRNA, featuring an extrahelical unpaired cytosine [5].

Junctions: Branched nucleic acid species, or junctions, are common characteristics in higher-order RNA structures. They are present when multiple arms of tRNAs or rRNAs are present (Figure 2.9), and play an important role in the

global folding of RNA structures as well as protein recognition and enzymatic processes.

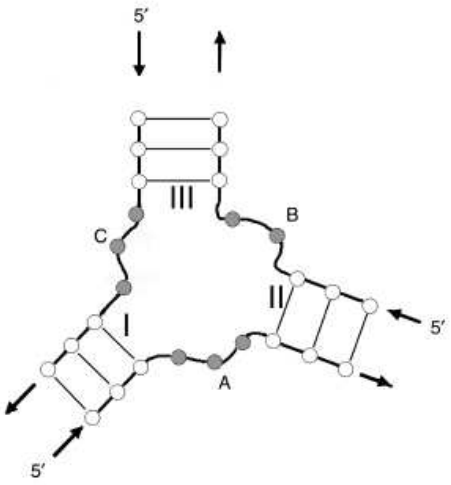

FIGURE 2.9. Schematic drawing of a three-way junction [14].

Kissing hairpins: they are the result of interactions between secondary structural elements, and sometimes called “tertiary structure” of nucleic acids. Kissing hairpins (Figure 2.10) occur when unpaired bases of one hairpin loop pair up with those of another. “Tertiary structure” also include pseudoknots, consisting of two stem-loop structures in which the loop of the first forms part of the stem of the second; and myriad loop–loop, bulge–loop, and bulge–bulge interactions.

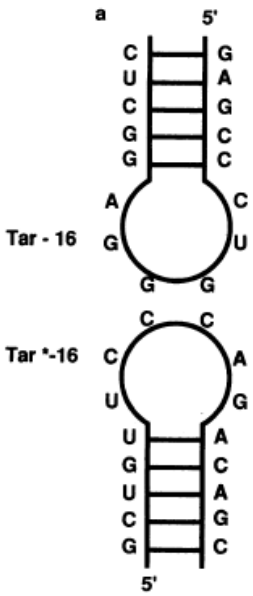

FIGURE 2.10. Schematic drawing of a kissing complex between hairpins TAR-16 and TAR*-16 [15]. Kissing complex derived from the HIV genome.

2.2 INTERACTION OF NUCLEIC ACIDS WITH DIVALENT IONS

The nucleic acids are polyions charged negatively; this negative charge is carried mainly by the phosphate groups. In order to form stable structures, nucleic acid needs the help of external molecules to neutralize its charge.

For the DNA of higher organisms this neutralization is mainly carried out by specialized basic proteins (the histones). In other nucleic acids such as chloroplast and mitochondrial RNA and DNA, or in mono-, di- or triphosphate nucleotides found as monomer units in the cellular medium, this function may be performed by metal ions. Metal ions may also stabilize the nucleic acids of bacteria and viruses.

Certain ions are much more effective than others promoting the stabilization of nucleic acid structures; this stabilization depends on the concentration of the ions. Studies have shown that some cations can induce precipitation of nucleic acids and interact with bases to promote destabilization of secondary structures.

The binding of metal ions to nucleic acids has been subject of study for many years, but the mechanism of their action is still mostly unknown. It is expected that the primary interaction of positive ions towards the stabilization of the nucleic acid structures is the interaction with the negatively charged oxygens of phosphate groups of the backbone. However, the positively charged metal ions may also interact with other sites characterized by high electron density or negatively charged residues like the electron donor atoms of the bases, such as N and O (see Figure 2.11.). Studies have shown that recurrent sites of cation binding to nucleotides are the base ring nitrogens, and the exocyclic base keto groups like N7 and O6 of guanine and N7 and N1 of adenine bases and the N3 of pyrimidines. Other potential sites for binding of metal ions are the ribose hydroxyls.

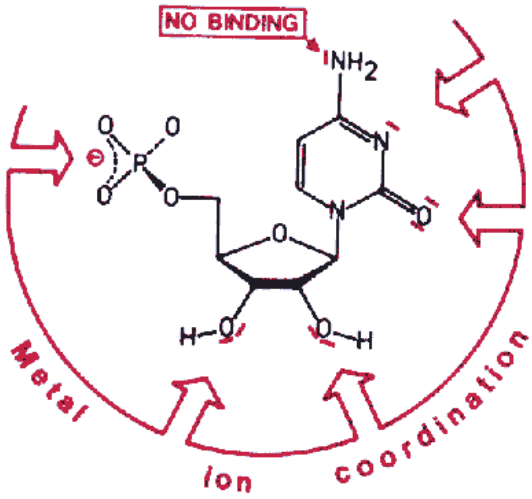

FIGURE 2.11. Schematic description of possible metal ion coordination sites on a nucleotide [1].

All this allows understanding the preferential localization of cations at some sequences, and the non-uniform distribution of these cations along a nucleotide polymer in solution. The binding of metals to nucleotides or polynucleotides does influence the sugar conformation and then, it may change the helical conformations.

The stabilization or destabilization of the nucleic acids structures may take place through water molecules (secondary coordination sphere, long-range electrostatic Coulombic interaction) or with a higher energetic cost it may involve direct coordination (internal coordination sphere, chelating of ions). For example, Magnesium ions are hydrolyzed in water and exist as a ‘free’ hexahydrated cation (Figure 2.12).

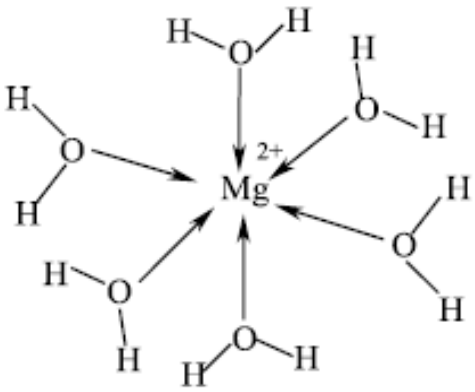

FIGURE 2.12. Scheme of the ‘free’ magnesium ion in water.

The higher cost of the internal coordination sphere interaction is due to the desolvating of the ion and of the nucleic acid. The transition metals can lose their water molecules very easily and give inner sphere coordinated complexes. Among the alkaline earth metals Ca^{2+}, Sr^{2+} and Ba^{2+} usually interact with nucleic acids in an inner sphere manner. The two most common inorganic cations present in the intracellular medium, K^{+} and Mg^{2+}, are usually engaged in more outer-sphere complexes, because of its stability and higher Gibbs free energy of hydration. Other metal ions such as Mn^{2+}, Cd^{2+} and Pb^{2+} have *d*-electrons and/or high polarizability which promote covalent bonding. These metals tend to bind nucleic acids more strongly than Mg^{2+} or K^{+} do.

The grooves in the nucleic acid helical structures are flexible and their flexibility responds to cation binding, the groove width changes with the position of bound cations. In the case of divalent cations like magnesium, a narrow minor groove of a nucleotide double stranded helix may be related to ion binding near the top of the groove, with the waters of its hydration shell often bridging the two phosphate backbones. A wide minor groove is associated with divalent ions that have penetrated deep into the groove, with their first shell of hydration intact. In the case of major grooves, the ways of binding of a hydrated divalent cation (with a size ~5–7 Å) are analogous to those of the minor grooves, but the first way of binding is possible only for A-form because of the shorter distance between phosphate groups on the top of the major groove compared with that of the B-form [16, 17].

The preferential localization of cations is inside the minor groove of some AT-rich sequences and in the major groove of some GC-rich sequences, in the cases of long-range electrostatic interaction. The favorable entry of divalent cations is a result of a wide, very electronegative minor groove, which is a sequence-dependent phenomenon [16].

Magnesium and nucleic acids

Inorganic elements penetrate to organisms in the form of soluble ions. The average elemental composition of a human being is shown in Table 2.2. The metal ions present in the highest concentration in the human body are Ca(II) and Mg(II); Ca^{2+} ions have a structural function – they form endo- and exoskeletons, and ensure the integrity of cell membranes. Certain ions as Na(I), K(I), Ca(II) create an actively maintained transmembrane concentration gradient and via ion channels participate in the information transfer. Metallic cations as for example Zn(II) or Mg(II) play the role of Lewis acids and facilitate the formation, metabolism and degradation of organic compounds in the physiological pH [18, 19].

TABLE 2.2. Average elemental composition of a human body. Principal elements in the body of an adult of 70 kg. [19].

Element	Symbol	Mass (g)
oxygen	O	45500
carbon	C	12600
hydrogen	H	7000
nitrogen	N	2100
calcium	Ca	1050
phosphorus	P	700
sulfur	S	175
potassium	K	140
chlorine	Cl	105
sodium	Na	105
magnesium	Mg	35
iron	Fe	4.2
zinc	Zn	2.3

The divalent alkaline earth metals are rather more reactive than alkali metals. They react as the alkali metals do and more. From the alkaline earth metals magnesium is the divalent ion with major presence in the intracellular space, even when its

physiological concentration (around 10mM) is low compare with the physiological monovalent cation concentrations (0.1-0.2 M).

The capability of stabilization of nucleotide structures depends of the type of cation. Milimolar Mg^{2+} concentrations can stabilize nucleotide tertiary structures that are otherwise only marginally stable in the presence of high monovalent cation concentrations. This property of magnesium was found almost 40 years ago by studying tRNA folding [20]. The possibility that Mg^{2+} also participates directly in the catalytic mechanisms of ribozymes [21] has made important the study of ion interactions with nucleotides and particularly with RNA.

Between the reasons of the effectiveness of Mg^{2+} in stabilizing nucleotide structures is that Mg^{2+} as divalent ion can coordinate with mono- and bi-dentate ligands and reduce the electrostatic stress arising from closely packed phosphates to about the same extent as two monovalent ions, but at a lower entropic cost because fewer ions are confined near the nucleic acid structure, meaning that there would be smaller repulsive electrostatic forces between each of the ions forming the cloud of cations around the structure where the ions respond to each other's presence through long-range electrostatic interactions [17; 22]. This results in substantially higher shielding effectivity of Mg^{2+} ions over monovalent ones at situation of densely packed nucleic chains, e.g. at the surfaces of biosensors [23].

About the possibility of direct binding of magnesium to nucleic acids, it must account the very high energetic cost of removing the water spheres necessary for the magnesium ion chelation. The large unfavorable free energies may be compensated by the strong interactions between the chelated Mg^{2+} and the nucleic acid structure, mainly due to the electrostatic interaction between the Mg^{2+} ionic charge and the nucleic acid electrostatic field. It is important to notice that the type of the complexes that magnesium can form is time, temperature and nucleotide-sequence dependent.

2.3 THE AIMS OF THE THESIS AND THE INTERESTING STRUCTURAL MOTIFS CHOSEN FOR THE STUDY OF MAGNESIUM INTERACTIONS.

The triple and double helices of nucleic acids are subjects of many researches in order to design oligonucleotides that will recognize unique base sequences and form stable complexes in the selected region. For making possible this idea, and for its posterior use in pharmaceutical applications, the rules of the association and the interaction between different units of the polymer, as well as the interaction of the triplexes and duplexes with the surrounding cations in solution need to be reliably understood.

The aim of this thesis is to study the details of magnesium ions interaction on selected nucleic acid structures. Raman spectroscopy was chosen as the basic experimental method to achieve this goal, due to its applicability for comparative studies of biomolecular solutions at varied conditions and the reach information content. To obtain the maximal spectral details, obtained series of Raman spectra were treated by factor analysis.

Complementary RNA and DNA homopolynucleotides, polyA plus polyU and polydA and polydT, able to form both duplex and triplex (Y.R:Y motif) structures, were chosen as the first group of studied nucleic acid molecular models. These molecular systems possess relatively simple Raman spectra due to the limited number of involved nucleobases. On the other hand, their can exhibit different morphological forms – besides the single strand, duplex and triplex form, at least polydA-polydT duplex can exist in two different B-like conformation. In all cases the equilibrium between possible forms depends strongly on environmental conditions, besides the sample temperature and the concentration ratios mainly just on the presence of particular metal cations.

The second studied molecular model was the apical hairpin-loop of TAR segment of HIV-1 RNA genome. This hairpin is a potential target for aptamer therapeutical treatment based on an inhibition of the binding site for viral Tat protein at the loop via kissing complex formation with an aptamer. For a successful complexation,

presence of several mM Mg^{2+} is considered as indispensable. This brings about the natural question of the magnesium role in the formation of the hairpin structure and its stability.

2.4 STRUCTURAL PROPERTIES OF COMPLEXES FORMED BY PolyA AND PolyU.

In equimolar mixtures of polyA and polyU a right-handed double helix is formed at neutral pH in solutions of low or moderate monovalent cation concentration. Under similar conditions when the ratio of poly(U)/poly(A) exceeds 1.0, the formation of a particular complex between two strands of polyU and one strand of polyA is formed. This three-stranded right-handed helix was the first triple helix structure detected [24].

The stability of these two complexes and their thermal properties (Table 2.3) depend upon the cation concentration in the solution. Although both complexes of polyU and polyA have been extensively studied and the molecular details of their helical structures have been early defined by fiber x-ray diffraction studies [25], the influence of divalent cations on the structural properties of these complexes is not yet completely understood.

TABLE 2.3. Thermodynamic parameters for polynucleotides.

Polymer	Tm, °C	ΔH_{Tm}, kcal/mol
§ AU – A + U	61.79 ± 0.01	8.074 ± 0.030
AT – A + T	*58.2 ± 0.5 § 73.07 ± 0.02	* 9.36 ± 0.28 § 8.257 ± 0.040
$^{\Delta}$ TAT – A + 2T	87.61 ± 0.01	13.420 ± 0.130
$^{\delta}$ UAU – A + 2U	77.80 ± 0.01	10.530 ± 0.060

$^{\gamma}$ 170 mM NaCl + 0.01M Na cacodylate, pH 7.0 [27].
* 32 mM NaCl + 0.01M Na cacodylate, pH 6.8 + 0.1 mM Na_2EDTA.[26].
$^{\Delta}$ 1.13 M NaCl + 0.01M Na cacodylate, pH 7.0 [27].
$^{\delta}$ 1.28 M NaCl + 0.01M Na cacodylate, pH 7.0 [27].

The first detection of the polyA-polyU-polyA triplex was done in the presence of Mg^{2+} [24] and from then diagrams for the conformational equilibrium of single-, double- and three-stranded structures in polyA-polyU and polyA(2polyU) solutions

have been obtained at Mg^{2+} ion concentrations of 10^{-5} – 10^{-2} M in the range of temperatures 20-96 ºC [28].

2.5 STRUCTURAL PROPERTIES OF COMPLEXES FORMED BY PolydA AND PolydT.

PolydA-polydT polynucleotides have considerable structural rigidity compared with other polynucleotides. Most DNA sequences are able to change from B-DNA to A-DNA on reducing the humidity, but polydA-polydT does not undergo this transition. They can not be classified as either A-DNA or B-DNA, their structural and functional properties classified them as a B'-DNA form [29]. The two polynucleotide chains have different conformations; the polydA chain is more like A-DNA (3'-endo pucker), whereas the polydT chain is more like B-DNA (2'-endopucker).

The structural rigidity of polydA-polydT arises from a high propeller twist of the base pairs, which improves the interaction between adjacent bases [4]. This also creates a system of bifurcated hydrogen bonds within the DNA major groove in which N6 of adenine is close to O4 of the thymine on its 3'-end side [30].

Using X-ray fiber diffraction, Premilat and Albiser [31] observed a reversible temperature-dependent conformational transition for polydA-polydT with a midpoint at 30ºC. The low-temperature structure is less straight with more bifurcated hydrogen bonds in the major groove. When the temperature increases, there are changes in the thymine C4=O stretch and in the adenine N6 amino scissor mode detected by UV Resonance Raman that suggested the breaking of the bifurcated hydrogen bonds and the appearance of the structure that is more straight and more similar to the B-DNA conformation, with a wider minor groove and less propeller twisting of the base pairs [31].

By analogy with the A-T-rich double-helical DNA, the triple-helical polydT-polydA-polydT B form should be called the B' form of triple helical DNA. It has 12 residues per turn and an axial rise per residue of h= 3.26 Å. The in vivo role of polydT-polydA-polydT triplexes has been studied in relation with the possible

intermolecular formation of such triplexes in some A_n tracts on nucleosomal DNA where, due to their rigidity, can be resistant to nuclease attack and intercalative drug binding [30].

2.6 STRUCTURAL PROPERTIES OF TAR HAIRPIN.

Other model studied was the 14-mer hairpin loop of the TAR element. The trans-activation response (TAR) element of human immunodeficiency virus-1 (HIV-1) RNA is a 59-nucleotide chain of RNA in a stem-loop structure near the 5'- end of HIV-1 transcripts. TAR serves as the binding site of the viral Tat protein. It has been found that the TAR-Tat complex greatly enhances the viral transcription. The TAR element presents a 3 nucleotide bulge and a 6 nucleotide hairpin loop (see Figure 2.13). The Tat protein specifically targets the site of a three-base bulge (either UCU or UUU) on the stem of the TAR element, most likely due to the increased flexibility and more open major groove in this region (Figure 2.13).

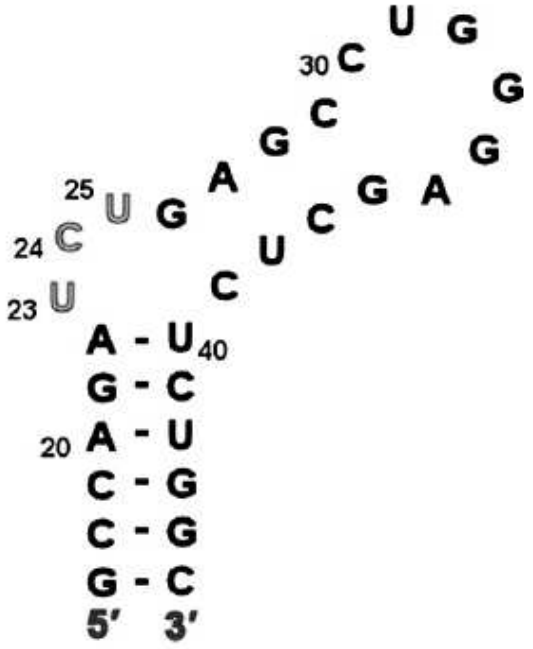

FIGURE 2.13. Sequence of the TAT binding site of HIV-1 TAR RNA [5]. The unpaired bulge nucleotides are numbered 23–25.

Fluorescence studies also provide evidence for Mg^{2+} destabilizing complexes of TAR with Tat-derived peptides [32]. Mg^{2+} has been found to bind specifically to the bulge region of the TAR RNA hairpin by NMR [33] and 19F NMR spectroscopy [34]. In the Olejniczak et al.'s work [34] very weak chemical shifts of the labeled uracil 31 of the apical loop were detected with the magnesium addition. These studies also present results obtained by RNA cleavages and computational simulations that support the idea of very weak interactions of magnesium ions with atoms of the apical loop.

Mutational studies conducted with HIV-1 TAR have demonstrated that the sequence of bases in the loop is not significant in comparison to certain stem and bulge sequences; however the overall hairpin structure is still necessary for efficient protein binding [35 - 37].

3. EXPERIMENTAL

3.1 SAMPLES

Single strand polynucleotides polyA, polyU, polydA and polydT, prepared as potassium salts, and double stranded polyUpolyA and polydTpolydA prepared as sodium salts, were purchased from Sigma-Aldrich.

The polynucleotides salts were dissolved in 80mM cacodylate buffer (pH 6.4). The concentrations of the polynucleotide stock solutions were 40 mM (in nucleotide monomers). For the experiments with double strands and triple strands polynucleotides, the solutions were heated up to 90℃ and slowly cooled down (during 12 hours) to room temperature.

Six (or three, in the case of the experiments with polydA and polydT) titration solutions containing $MgCl_2$ in concentrations of 0, 10, 20, 30, 40 and 50 mM (for the systems with polydA and polydT the $MgCl_2$ concentrations were 0, 5 and 10 mM) were prepared in 80mM cacodylate buffer. NaCl was added to the solutions in the concentrations to adjust the ionic strength of all solutions at the same value of 200 mM. Samples for the Raman titration experiment were prepared by mixing equimolar volumes of the six $MgCl_2$ titration solutions and the corresponding polynucleotide solution. So, the final concentration of magnesium and of each polynucleotide (and the ionic strength of the solution) was reduced to the half.

RNA oligonucleotide of 5’-GAGC-CUGGGA-GCUC-3’ sequence that forms the apical TAR hairpin was synthesized, 2’-deprotected, desalted, and PAGE purified by Dharmacon (USA). For the Raman measurements, the oligonucleotide was dissolved in 20 mM sodium cacodylate buffer containing 140 mM KCl and 20 mM

NaCl. The pH of the buffer was set to 6.4. Two samples, the first one without magnesium and the second one with 6 mM Mg^{2+} ions added as $MgCl_2$, were measured. The oligonucleotide concentration was 1.4 mM in both cases.

For UV absorption measurements, three samples of 7.5 μM per oligonucleotide of TAR hairpin dissolved in the same buffer (20 mM sodium cacodylate buffer containing 140 mM KCl and 20 mM NaCl) were prepared: the first one without magnesium and other two with 3mM and 6 mM Mg^{2+} ions added as $MgCl_2$.

3.2 RAMAN EXPERIMENTS.

Raman spectra were excited by the 532.15 nm line of a Nd-YAG Verdi V2 laser (Coherent) with the power at the sample of around 0.5W. Spectra were measured using a 90° scattering geometry (the schematic repr esentation of the experimental setup is shown in Figure 3.1) by a Spex 270M spectrograph (Jobin-Yvon) with 1800 grooves/mm grating and a liquid nitrogen cooled CCD 1340 × 100 detector (Princeton Instruments). Raman shifts of the sample spectra were calibrated by using Raman spectra of a neon lamp recorded after each measurement of the sample.

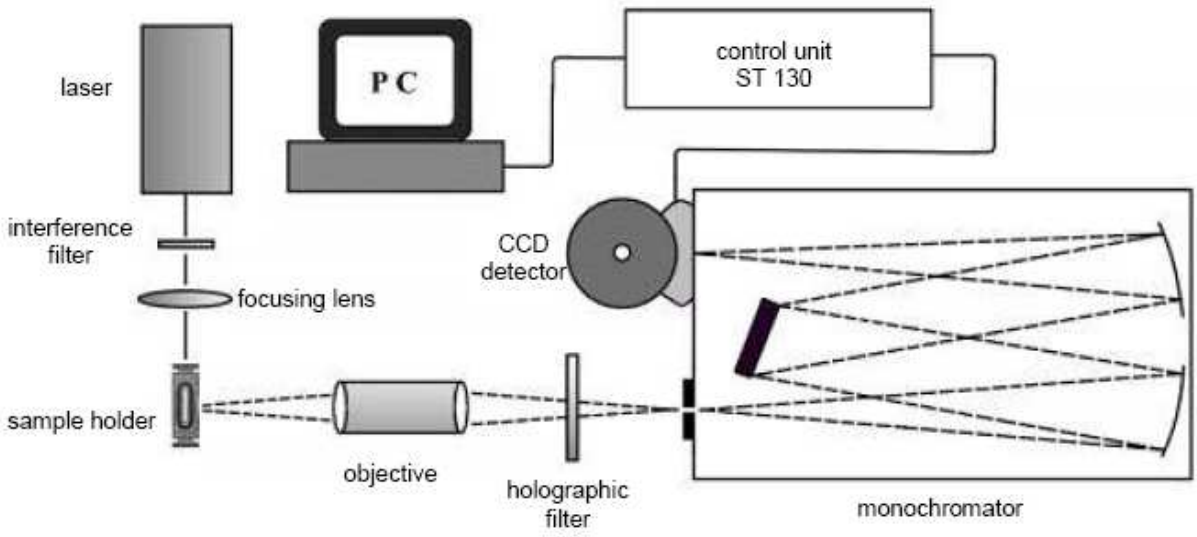

FIGURE 3.1. Schematic representation of the experimental setup for the Raman-Spectroscopy experiments [38].

Raman spectra of the systems formed by polyA and polyU were measure in a 10ul microcell. Total acquisition times were 25min, temperature was stabilized at 18℃. Raman experiments carried out for the systems with polydA and polydT and with the TAR hairpin were more extensive because at each magnesium concentration, Raman spectral series were recorded in the temperature range from 10℃ to 90℃, with steps of 10℃ for the polynucleotide systems and with 5℃ steps in the case of the TAR hairpin. These temperature-dependence Raman spectra were measured in an even smaller microcell with 4 µl volume. Total acquisition times were around 20 minutes and the sample temperature was stabilized for 15 minutes before each measurement.

The capillary microcells (of 10 and 4 µl) for the Raman spectra measurements were placed in a cooper cell holder built in the lab. It allows the control of the sample temperature with a stability of 0.1℃ (Figure 3.2). The cell holder was thermally isolated from the environment by Teflon housing.

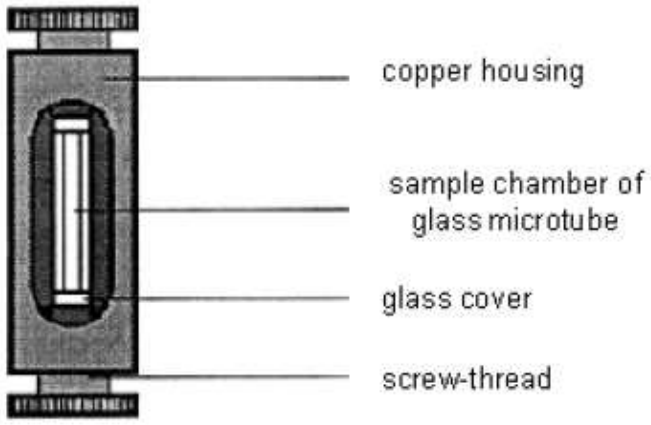

FIGURE 3.2. Schema of the microcell inside the holder.

3.3 TREATMENT OF RAMAN DATA.

Background correction was performed by subtracting water and cacodylate Raman spectra and by subtracting a fifth degree polynomial. The spectra were normalized using the water band at 1640 cm^{-1} as an internal standard.

3.3.2. Factor analysis

The most of sets of Raman spectra after the background correction and normalized to water were subjected to factor analysis by using a singular value decomposition (SVD) algorithm. It decomposes a set of N spectra, $Y_i(\nu)$, $i=1,\ldots,N$, into a set of independent (but artificial) orthonormal spectral components

$$Y_i(\nu) = \sum_{j=1}^{N} W_j V_{ij} S_j(\nu) \tag{3.1}$$

$$\sum_{\nu} S_j(\nu) S_k(\nu) = \delta_{jk} \tag{3.2}$$

The coefficients V_{ij} quotes relative portion of the j-th spectral component $S_j(\nu)$ in the i-th original spectrum $Y_i(\nu)$. They fulfil relations of orthonormality

$$\sum_{i=1}^{N} V_{ij} V_{ik} = \delta_{jk} \quad , \quad \sum_{j=1}^{N} V_{ij} V_{lj} = \delta_{il} \quad . \tag{3.3}$$

The singular number W_j stands for the statistical weight of the j-th spectral component. The factor dimension M $(M<N)$ represents the minimum number of components $S_j(\nu)$ that are necessary to make a good approximation of the original spectral set:

$$Y_i(\nu) \approx \sum_{j=1}^{M} W_j V_{ij} S_j(\nu) \qquad . \tag{3.4}$$

Singular values are created in an order of successive decreasing values:

$$W_k \leq W_l \text{ for } k > l \, . \tag{3.5}$$

Figure 3.3 illustrates how the SVD algorithm works. The obtained Raman spectra after background correction and normalization to the water band are shown in

Figure 3.3,a, where the points corresponding to zero intensity levels were separated for a better visualization. After applying the SVD algorithm, the terms occurring at the right side of eq. 3.1 were obtained (they are graphically represented in Fig. 3.3).

The Singular Numbers, W_j (Figure 3.3, b) allow the determination of the factor dimension. Higher value of singular number means higher importance. The values of Singular Numbers close to zero means components that represent noise and statistically not significant artifacts such as incomplete background or solvent subtraction.

When the Raman spectra are normalized, the coefficients corresponding to the first component, V_{i1}, also called the First coefficients, often take almost the same value for all the data because the first subspectrum $S_1(\nu)$, which is of the highest statistical weight W_1, represents an average spectrum of the set of the experimental spectra. The changes due to temperature or concentration of ions are then mainly visualized in the second and higher order spectral components. The second subspectrum $S_2(\nu)$ describes the average difference between the experimental spectra and $S_1(\nu)$, the third subspectrum $S_3(\nu)$ indicates the average difference between the experimental spectra and the optimal linear combination of $S_1(\nu)$ and $S_2(\nu)$, etc.

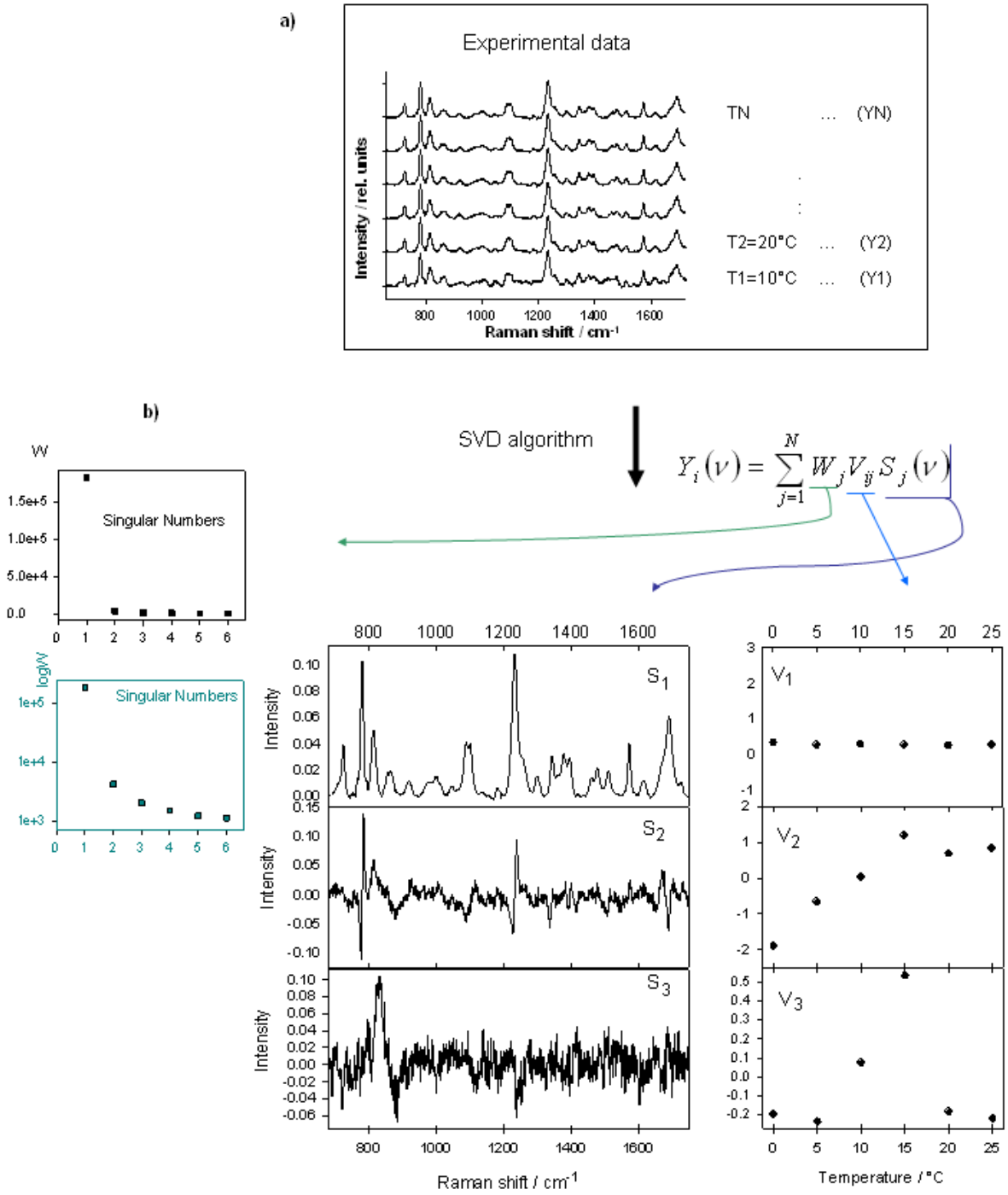

FIGURE 3.3. Result of Factor analysis applied to a set of Raman spectra of polynucleotides at different temperatures. a) Background-corrected and normalized Raman spectra, $Y_i(\nu)$. b) Singular Numbers, W_j, note that the first spectral component is two orders of magnitude higher than the rest. S_1-S_3) First three spectral components, $S_j(\nu)$.V_1-V_3) Coefficients, V_{ij}, relating each of the three shown spectral components, $S_j(\nu)$, to each one of the original spectra, $Y_i(\nu)$.

3.3.2. Determination of stability constants

According to eq.3.4, experimental Raman spectra can be approximated as linear combinations of the factor analysis spectral components (subspectra). As Raman scattering fulfils a superposition law, each experimental spectrum $Y_i(\nu)$, $i = 1$,…, N can be written as a linear combination of the spectra of individual species $Z_j(\nu)$, $j = 1$,…, L (L is their total) in the sample:

$$Y_i(\nu) = \sum_{j=1}^{L} C_{ij} Z_j(\nu) \quad , \tag{3.6}$$

where C_{ij} represents the molar concentration of the j -th species in the i -th sample. The spectra of pure species $Z_j(\nu)$ are given in terms of normalized intensities corresponding to a unit concentration of the compound. The values of C_{ij} can often be given by equilibrium equations as a function of stability constants and total concentrations of the interacting compounds.

In the same way as the experimental spectra, the spectra of pure species $Z_j(\nu)$ can be expressed by linear combination of M SVD subspectra $S_j(\nu)$:

$$Z_i(\nu) = \sum_{j=1}^{M} R_{ij} S_j(\nu) \quad , \tag{3.7}$$

where $\mathbf{R}$ represents the transformation matrix. If no artifacts are present in the experimental spectra, the factor dimension M is equal to the number of individual compounds L and thus $\mathbf{R}$ is a square matrix.

Substituting (3.7) to (3.6), taking into account the approximation of the experimental spectra (3.4) and the relations of orthonormality (3.2), we obtain for the transformation matrix $\mathbf{R}$:

$$\sum_{k=1}^{L} C_{ik} R_{kj} = W_j V_{ij} \qquad \text{for } i = 1,\ldots, N \text{ and } j = 1,\ldots, M \quad . \tag{3.8}$$

This relation represents a set of $N \times M$ linear equations for the components of the transformation matrix $\mathbf{R}$ and of the concentration matrix $\mathbf{C}$. As the components of $\mathbf{C}$ are determined by the equilibrium equations, a least-square fit of eq. 3.8 can provide the values of the stability constants in addition to the components of the transformation matrix $\mathbf{R}$. Afterwards the spectra of pure species can be calculated with the help of eq. 3.7. If we consider the relations of orthonormality (3.3) we can rewrite eq. (3.1) in the following way:

$$S_j(\nu) = \frac{1}{W_j} \sum_{i=1}^{N} V_{ij} Y_i(\nu) \qquad \text{for } j = 1,\ldots, N \qquad (3.9)$$

Substituting (3.9) into (3.7) the spectra of individual components can also be constructed as:

$$Z_k(\nu) = \sum_{j=1}^{M} \sum_{i=1}^{N} \frac{R_{kj}}{W_j} V_{ij} Y_i(\nu) \qquad \text{for } k = 1,\ldots, L. \qquad (3.10)$$

3.4 UV ABSORPTION.

Temperature-dependence UV absorption spectra were recorded for the TAR samples on a commercial two-beam UV-VIS spectrophotometer Lambda 12 (Perkin Elmer), in the spectral region of 220–340 nm and in the temperature range from 10℃ to 90℃, with steps of approximately 3℃. The spectra were also analyzed by factor analysis.

4. RESULTS AND DISCUSSION.

4.1 PolyA- PolyU SYSTEMS.

Detailed studies of magnesium ion interactions with model nucleic-acid structures, performed within the thesis, had started on the system of polyadenylic-polyuridylic acid systems as following up an investigation of the influence of several divalent metal cations on these systems. In Hrabáková's MSc. diploma thesis [38], three different cations were chosen: copper, nickel and magnesium, and temperature dependence of the Raman spectra were recorded in the range of 20–80℃. The observed effect on the stabilization of the polyA-polyU duplex system was almost equal for nickel and magnesium ions, increasing the melting temperature (the copper ions did not seem to interact with the complex). However, in mixtures of triplex and duplex structures interestingly magnesium ions showed a preference for the stabilization of the triplexes over the duplexes, and a probably formation of triplexes from melted duplexes was suggested (equation 4.1).

$$polyA \cdot polyU + polyA \cdot polyU \rightarrow (polyA \cdot polyU) \cdot polyU + polyA \qquad (4.1)$$

The same year, Kankia [39] by less structurally sensitive methods found that increased magnesium concentration in a mixed solution of polyU and polyA in 1:1 stoichiometric ratio can lead to decrease of duplexes concentration and at the same time appearance of triplexes. Kankia also found evidence of direct binding of Mg^{2+} to single-stranded polyA and polyU [40, 41] and suggested that a direct binding may happen in the triplexes.

4.1.1. Single stranded polyA and polyU

To begin our study on the complexes formed in solutions containing polyU and polyA, we have performed Raman magnesium titration experiments on solutions

containing only one type a polynucleotide. In this case the homopolynucleotide is in a more or less ordered single-stranded form (at neutral pH), in which the nucleobases are more accessible for binding of magnesium ions than in the case of duplex or triplex structures.

Spectra of polyU were measured in solutions containing various magnesium-ions concentrations in the range of from 0 to 25 mM. Raman spectra, as they were obtained directly from the spectrometer are shown in Figure 4.1. Basic character of the spectral profiles was typical for all Raman measurements on nucleic-acid solutions: the dominant peaks in the spectrum belong to the buffer (in case of the cacodylate buffer the highest peak is around 600 cm^{-1}) and to water (the widest band at 1640 cm^{-1}). Strong and medium nucleic-acid Raman bands are well resolvable in the original spectrum, but a good background correction is indispensable to obtain pure Raman spectrum of the species under study applicable for further analysis.

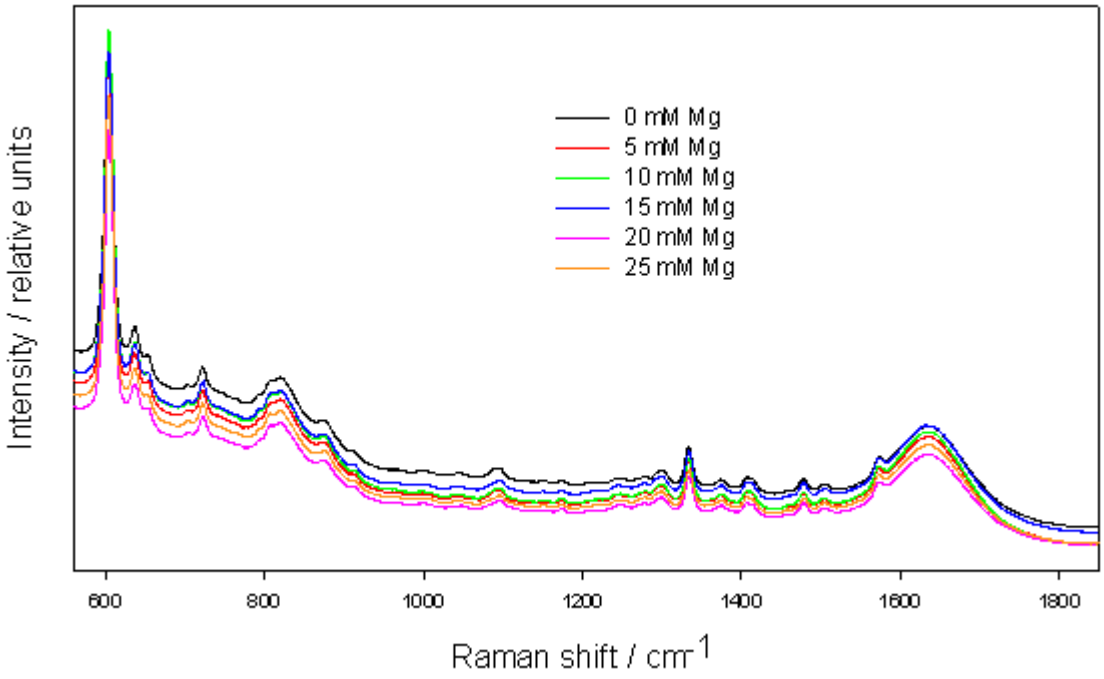

FIGURE 4.1. Original Raman spectra of 20 mM polyU in cacodylate buffer (pH 6.4) at different concentrations of magnesium ions, temperature 18℃.

For the background correction, Raman spectra both of the buffer and of pure water had to be measured at the same conditions as the basic nuclei-acid solutions. The background correction included subtraction of the buffer and water spectral profiles together with an arbitrary polynomial of fifth degree fitted to correct the smooth contributions in the spectrum caused by fluorescence or not completely eliminated elastic scattering. The spectra were also normalized by using the subtracted water band as an internal standard.

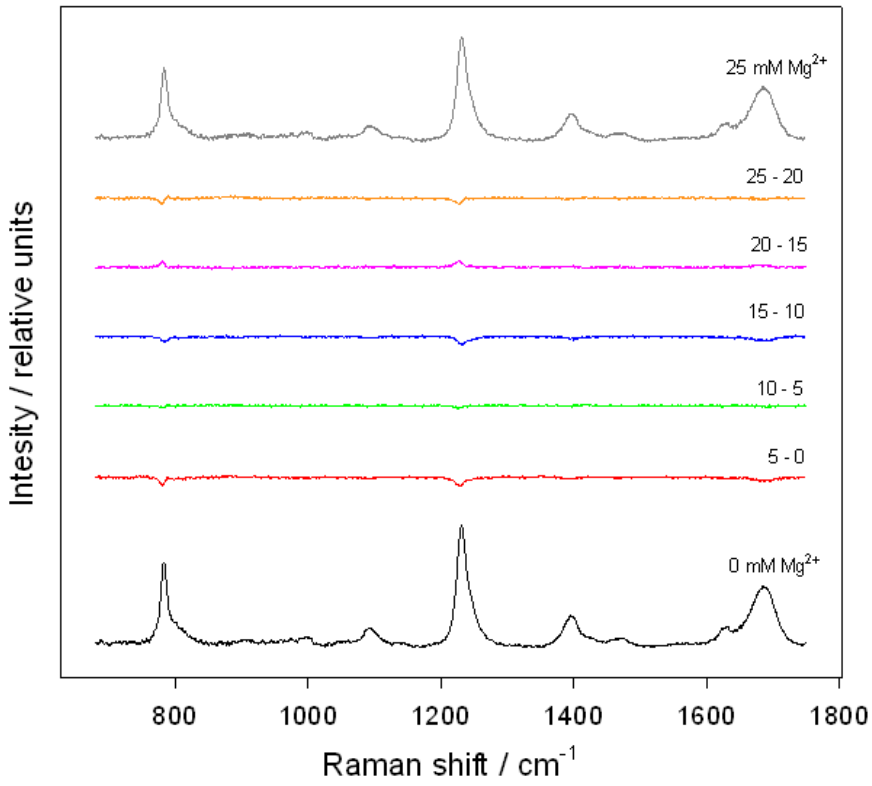

FIGURE 4.2. Background corrected Raman spectra of polyU in cacodylate buffer (pH 6.4) and their mutual differences for various magnesium concentrations, temperature 18℃.

The results of the background subtraction are shown in Figure 4.2 as Raman spectra obtained for the limit Mg^{2+} concentrations (0 and 25 mM) and mutual differences between spectra obtained at successive concentrations. As the main base for a quantitative analysis and/or interpretation of obtained spectra, we subjected the series of background corrected spectra to the factor analysis procedure (Singular Value Decomposition - SVD).

SVD results of the polyU spectra are shown in Figure 4.3. Singular values indicate that the factor dimension, i.e. the number of spectral components distinguishable in the spectral set, is two. The first component is dominant while the statistical weight of the second component represented by the second singular value is just above the noise level, and is visible only when the singular values are plot in a logarithmic scale. It means that changes of Mg^{2+} concentration influence weakly but detectably Raman spectrum of polyU. The terms of order higher than two contain mainly noise, which can be seen both from the profile of the spectral components and from the absence of any correlation between the related V coefficients values and concentration of magnesium ions (or any other possible influence like, for instance, the succession of measured samples).

The first coefficients display certain but very weak decrease of the overall intensity of Raman spectrum with increased concentration of magnesium ions. As in the case of polyU all strong Raman bands are hypochromic, it may be interpreted as a weak (not described in the literature), Mg^{2+} induced, rise of the uracil stacking. As polyU is known to be almost disordered at temperatures above 10℃, it means that presence of magnesium ions support certain preference of a temporary stacked mutual orientation of neighboring uracils. The second spectral component describes a weak spectral shift of the two strongest uracil Raman bands. This shift correlates with increased concentration of magnesium ions only partly. Very probably due to the very weak statistical weight of the second component, it is a resultant of mixed effects of the magnesium induced spectral shift and of the artifact caused by imprecision of spectral calibration.

Due to the weakness of the magnesium ions effect in the case of polyU, it is not practicable to analyze quantitatively the dependences of the SVD coefficients on the concentration of magnesium ions. If we accept that magnesium ions bind to polyU so strongly as indicate the binding parameters determined in [40], i.e. the equilibrium association constant $K = (0.7 \pm 0.2)\ 10^4\ M^{-1}$ for 20℃ and the average number of binding sites per nucleotide $n = 0.20 \pm 0.03$, the only explanation of the

very weak effect on Raman spectra we observed can be in a non-specific outer-sphere binding that might not affect the spectra remarkably.

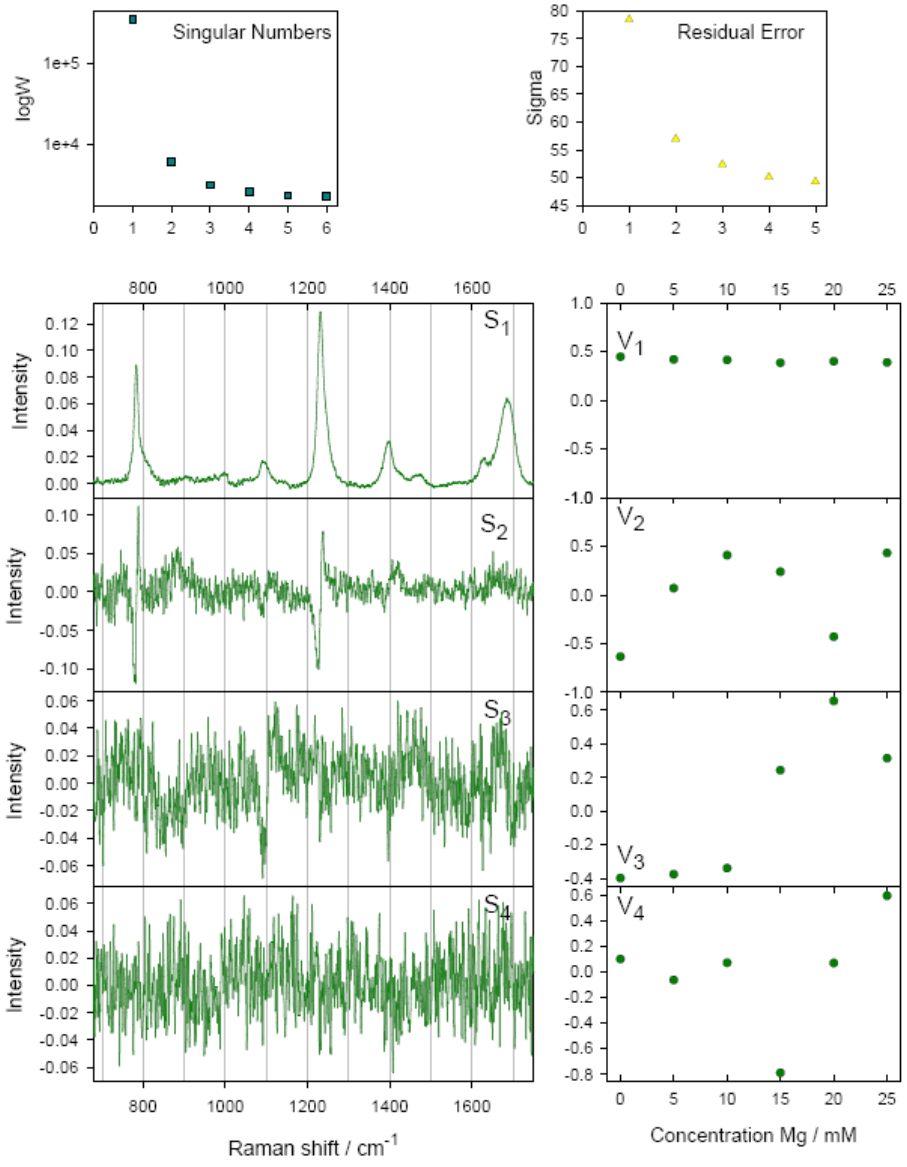

FIGURE 4.3. Results of Singular Value Decomposition applied to the set of polyU Raman spectra at various concentrations of magnesium ions shown in Figure 4.2.

In the case of polyA, the background corrected spectra and their differences are shown in Figure 4.4 for magnesium ions concentrations in the range of 0 – 10 mM.

Samples with concentrations of magnesium ions above 10 mM limit were not measured, because of magnesium-induced polyA precipitation [40].

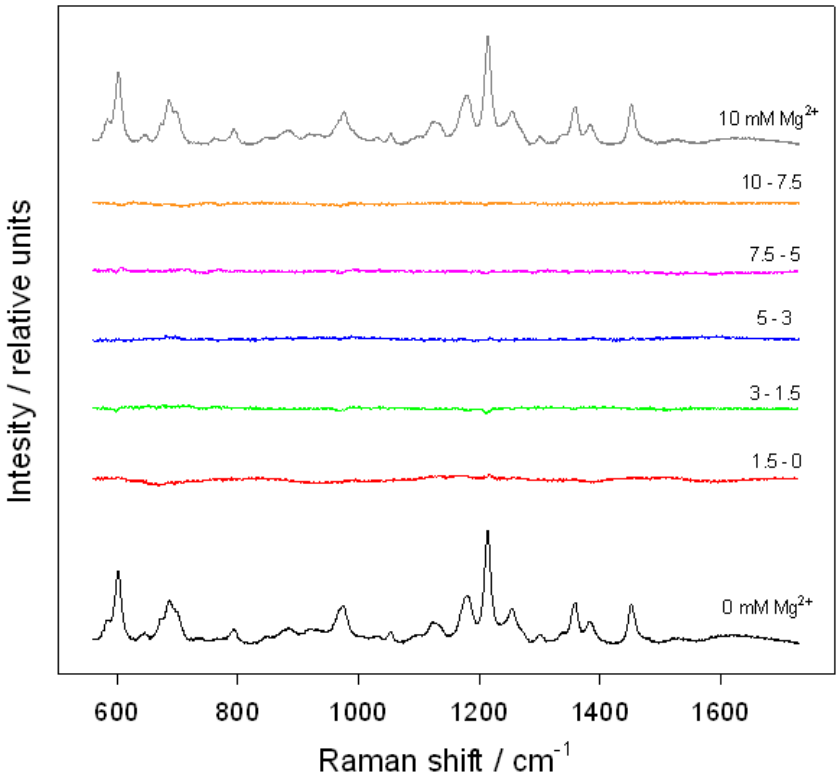

FIGURE 4.4. Background corrected Raman spectra of 20 mM polyA in cacodylate buffer (pH 6.4) and their mutual differences for various magnesium concentrations, temperature 18℃.

SVD results of the polyA spectra are shown in Figure 4.5. The factor dimension of the spectral set is again two. The contribution of the second component, evaluated by the ratio of the first and the second singular value, is though stronger than that of polyU.

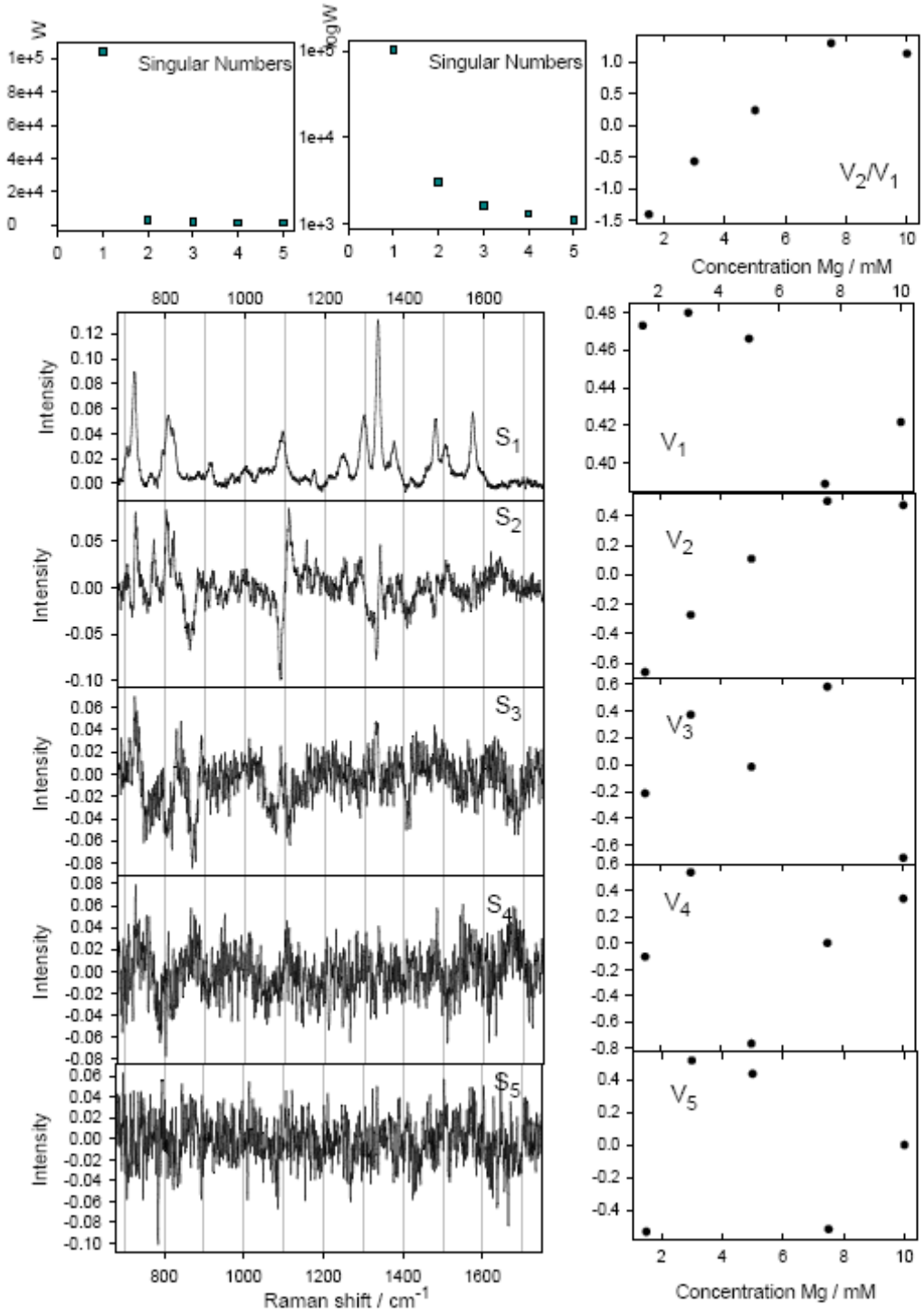

FIGURE 4.5. Results of Singular Value Decomposition applied to the set of polyA Raman spectra at various concentrations of magnesium ions shown in Figure 4.4.

The SVD results represent optimal reference data for further analysis of measurements on mixed solutions. For any magnesium concentration, relevant values of V_1 and V_2 can be estimated by interpolation of the obtained values. Spectrum of single-stranded polyA or polyU for this magnesium concentration (and temperature of 18℃) can be then constructed according to the formula (3.1), taking M=2 and the evaluated V_1 and V_2 values.

Looking at the literature data, we can summarize that different authors found out that magnesium ions increase stacking interaction of single stranded polyA, while no influence was observed on secondary structure of polydA, polyU and polydT [40-43]. The increase of magnesium concentration to 15 mM or higher values in polyA solution induces an aggregation/condensation process, which is also temperature dependent [40]. Our experience confirms the polyA precipitation for concentrations of magnesium ions above 10 mM (increased elastic scattering – data not shown). On the other hand, our results obtained for magnesium ions at lower concentrations are rather different. The effect of Mg^{2+} is mainly described by the second SVD spectral component as the coefficients corresponding to the first component are almost not affected by the changed magnesium concentration. The spectral shape of the second component shows that the main spectral change is connected with the upshift of the PO^- stretching vibration band around 1100 cm^{-1} indicating binding of magnesium ions to phosphates. The other spectral changes include the upshift of the adenine band at 1340 cm^{-1}, intensity increase and frequency upshift of the adenine breathing band around 730 cm^{-1}, and intensity increase of Raman bands in the region 800 – 820 cm^{-1} that are attributed to O-P-O stretching vibration of the diester bond, which is sensitive to torsional angles of the polynucleotide backbone.

We may conclude that the results of our Raman measurements do not sustain the outcomes of [40-43]; the changes in Raman spectra induced by magnesium ions are in the case of PolyA rather attributable to the magnesium binding than to the changed stacking interaction, while certain hypochromic effect is seen in Raman spectra of PolyU. In the latter case, the observed hypochromic effect may be

connected with the lower temperature of Raman measurements (18℃). The higher is the difference of the temperature from the temperature of polyU transition to a random-coil state (below 10℃), the more difficult is to restore stacked mutual orientation of uracil residues. In the former case, one can speculate about possible effect of different polyA concentration and/or effect of simultaneous presence of magnesium ions and highly concentrated monovalent ions (effect of sodium-magnesium competition).

Kankia [40] from acoustic and density measurements by analyzing the volume and compressibility effects of Mg^{2+} binding to polyA observed high dehydration effects, attributed to inner-sphere complex. From this analysis, the authors concluded that Mg^{2+} ions bind to polyA in a non-cooperative manner, the equilibrium association constant was determined as $K = (1.8 \pm 0.4)\ 10^4\ M^{-1}$ for 20℃ and the average number of binding sites per nucleotide $n = 0.26 \pm 0.04$. The amount of Mg^{2+} bound to polyA calculated according the above-mentioned binding parameters as a function of Mg^{2+} concentration shows also remarkable disagreement of our data, as at our conditions, practically all the Mg^{2+} binding sites at polyA should be occupied for 5 mM concentration of magnesium ions. This does obviously not correspond with the dependence of the second SVD coefficients (Figure 4.5) on Mg^{2+} concentration.

As our primary aim was to obtain reliable reference data for our Raman study of polyA-polyU duplexes and triplexes, we did not perform any additional more detailed experiments on single-stranded polyA and polyU, necessary to reveal the reason of the disagreement between our Raman results and those obtained by using other methods [40-43].

4.1.2. PolyA and polyU 1:1 mixtures

The results for the Raman magnesium titration of polyU and polyA mixed solution with 1:1 ratio of nucleotide concentrations are shown as SVD results in Figure 4.6.We can see, mainly from the spectral shape of the second spectral component and the dependence of its coefficients on the concentration of magnesium ions,

that the factor dimension of the spectral set is two. It means that within an experimental error the spectral effect of the gradually increased magnesium concentration can be again represented as a linear combination of only two spectral components. The first component represents some kind of an average spectrum with almost constant coefficients. The magnesium induced changes on the Raman spectra is thus represented just by the second component.

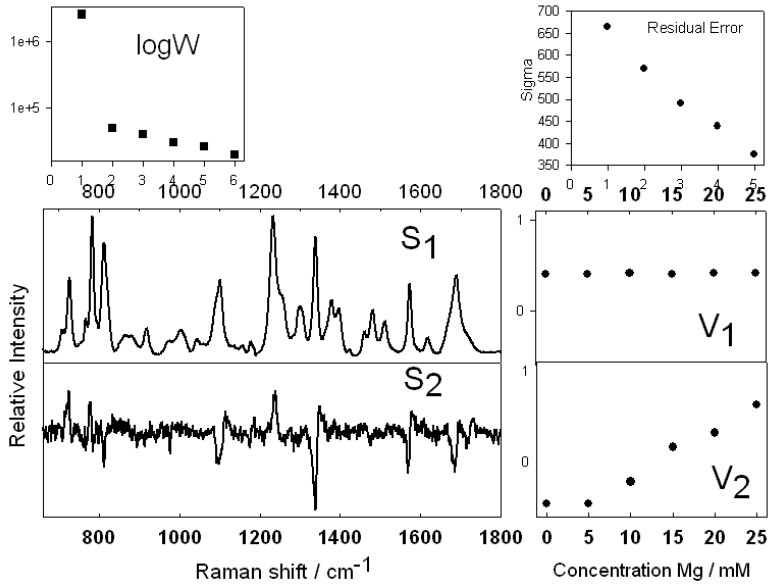

FIGURE 4.6. Results of Singular Value Decomposition applied to the Raman spectra set of 20 mM polyU-polyA in cacodylate buffer (pH 6.4) at various concentrations of magnesium ions, temperature 18℃.

Observed spectral changes given by the second spectral component are more intensive and different from those obtained when magnesium was added only to a single-strand polyU or polyA. Possible interpretation of the spectral changes is the magnesium induced triplex formation according to equation (4.1). Because it is known that Raman spectrum of polyU-polyA-polyU triplex differs sufficiently from any combination of polyU-polyA duplex, single-strand polyU, and single-strand polyA spectra [Hanus 1999], we can easily prove if the observed spectral changes agree with the expected magnesium induced reaction. Figure 4.7 compares the shape of the second SVD component with a calculated difference spectrum corresponding to the expected triplex formation from two polyA-polyU duplexes:

(polyA•polyU) • polyU + polyA − 2 × polyA•polyU .

(4.2)

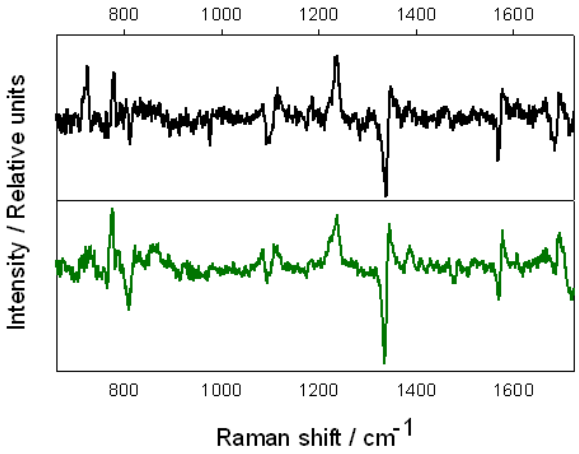

FIGURE 4.7. Evidence of the magnesium induced triplex formation from polyU-polyA duplexes. In black, the second SVD component obtained from the data analysis of Raman spectra measured from 1:1 mixed solutions of polyA and polyU at various magnesium concentrations. In green, the difference spectrum constructed mathematically from normalized Raman spectra obtained from solutions without magnesium according to equation (4.2)

High similarity of the two spectral profiles in Figure 4.7 clearly proves that the observed spectral changes really reflect the magnesium induced triplex formation from polyU-polyA duplexes. Because the difference spectrum was constructed from normalized Raman spectra obtained from solutions with the same nucleotide concentrations, we can also estimate the amounts of duplexes and triplexes in every 1:1 mixed solution of polyA-polyU. The results are shown in Figure 4.8. From the dependence of the duplex decrease and the triplex rise on the concentration of magnesium ions we can conclude that magnesium ions do not cause triplex formation until their concentration exceeds a half concentration of the duplex basepairs.

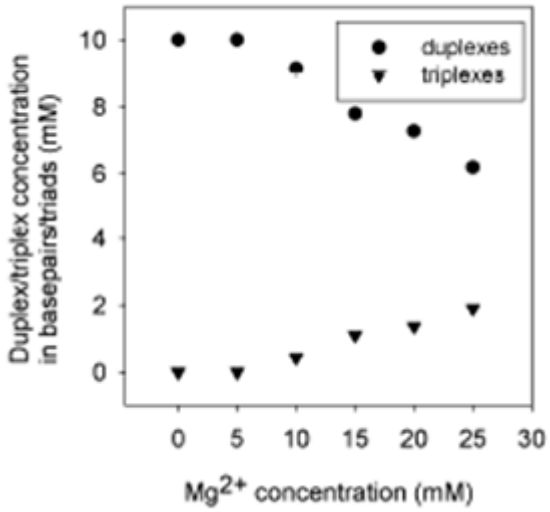

FIGURE 4.8. Estimated amounts of duplexes and triplexes present in the 1:1 mixed solution of polyU-polyA at various magnesium concentrations.

This result is the first evidence that Mg^{2+} ions induce formation of triple helices from polyA-polyU duplexes, detected with a technique directly sensitive to structural variations. It was published in Espinoza and Štěpánek [44]

4.1.3. PolyA and polyU 1:2 mixtures

The studies on polyA and polyU mixtures with 1:1 molar ratio were followed by experiments aimed to obtain Raman characteristics of the predicted specific binding of magnesium ions to the triple strands of polyU-polyA-polyU. Set of polyA-polyU mixed solutions with a 2:1 concentration ratio were prepared with different content of magnesium ions. In this case, it was expected that exclusively triplexes are formed in all samples and so the changes of Raman spectra should reflect only the direct effect of Mg^{2+} binding. The SVD results of the background corrected and normalized Raman spectra are shown in Figure 4.9.

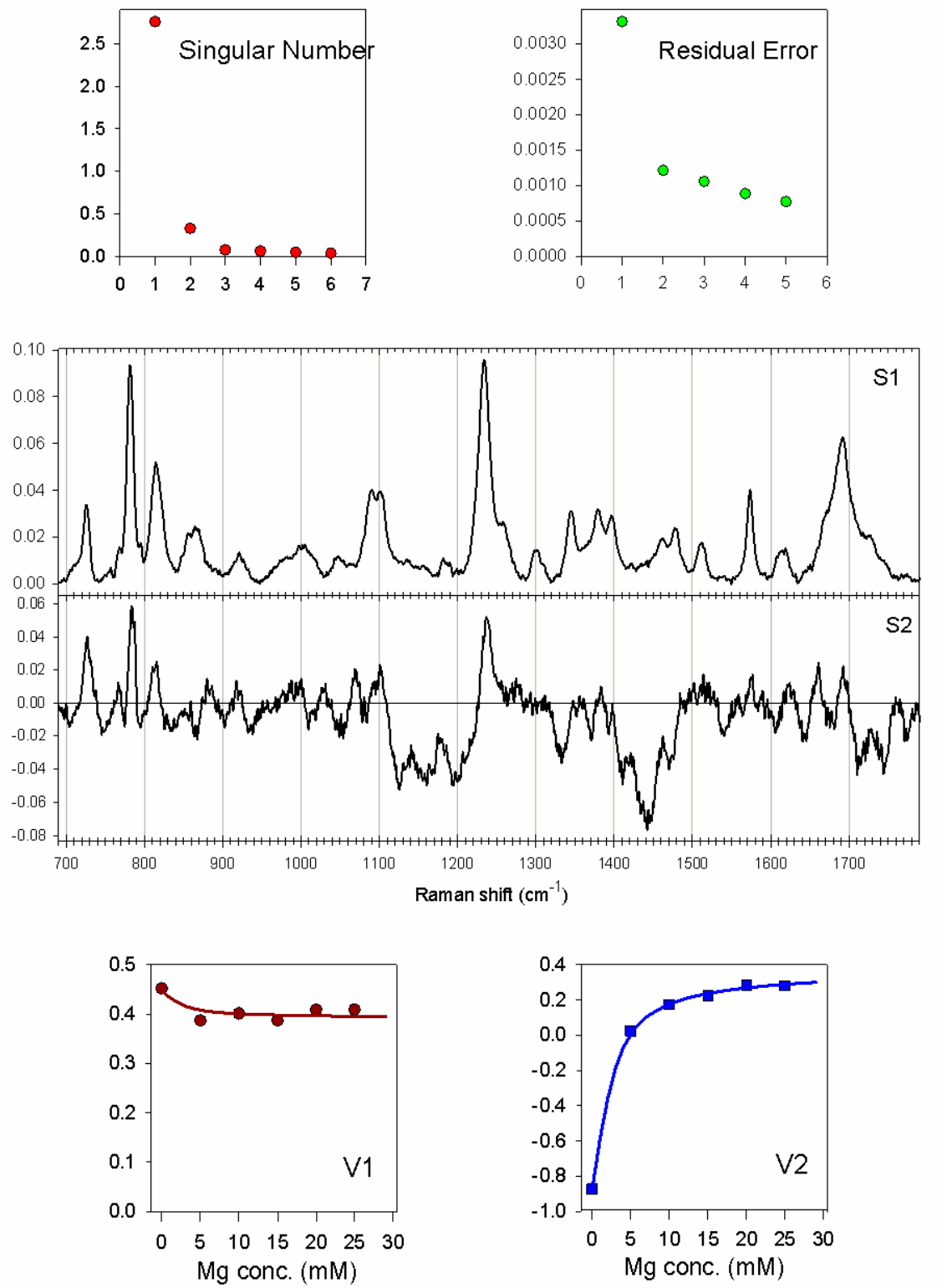

FIGURE 4.9. Results of Singular Value Decomposition applied to the Raman spectra set of 20 mM polyU-polyA-polyU in cacodylate buffer (pH 6.4) at various concentrations of magnesium ions, temperature 18℃. Solid lines in the graphs of V1 and V2 are results of the fitted McGhee-vonHippel model without cooperativity.

The factor dimension is again two. When magnesium ions are added to a solution that contains only RNA triplexes, the triplexes are more stable but do not change their amount or structure at room temperature. This enables the characterization of the magnesium binding to RNA triple strands. The second component reveals magnesium interaction with both kinds of bases as well as with the phosphate group that is different from that obtained in the cases of single-stranded polynucleotides or duplexes.

The dependences of the V1 and V2 coefficients on the concentration of magnesium ions were analyzed according to McGhee-von Hippel model [45]. This model considers simultaneous binding of numerous ligands to a polymer chain. If no cooperativity is considered, then the model provides relation:

$$rK_d = m(1-nr)\left(\frac{1-nr}{1-(n-1)r}\right)^{n-1} \quad , \qquad (4.3)$$

where r is the molar concentration of complexes divided by the total polymer concentration, m is the molar concentration of free ligand, n is number of polymer monomeric units required for binding of a single ligand and K_d is the equilibrium dissociation constant of the ligand binding. In our case molar concentration of polymer was expressed as molar concentration of U:A*U triads, i.e. it was 6.67 mM. r then means relative amount of triads bound to magnesium ion. m is concentration of free magnesium, i.e. $m = C_{Mg} - r \cdot 6.67mM$. K_d and n were estimated by a fit of the above mention relation simultaneously to both V1 and V2 by using relation (3.8). The fit was very good as shown by the solid lines in Figure4.9. The obtained values are:

$K_d = (1.1 \pm 0.3)\cdot 10^{-3}$ M

$n = 1.8 \pm 0.2$.

Next fit was performed by using the McGhee-von Hippel model considering cooperativity of the ligand binding. The relation is then

$$rK_d = m(1-nr)\left(1-\frac{2r}{1-(n-1)r+R}\right)^{(n-1)}\left(\frac{1-(n-1)r+R}{2(1-nr)}\right)^2 \quad , \qquad (4.4)$$

where $R = \sqrt{\left((1-(n-1)r)^2 + 4(\omega-1)(1-nr)\right)}$.

(4.5)

This fit was only slightly better, but the cooperativity parameter ω (=1 means no cooperativity, >1 cooperativity, and <1 anticooperativity) was impossible to be determined with a good precision. We can only conclude that there is none cooperativity of Mg^{2+} binding to polyA or the binding exhibits weak anticooperativity.

The obtained binding parameters with estimated precisions are:

$K_d = (1.0 \pm 0.3)\cdot 10^{-3}$ M ,

$n = 1.8 \pm 0.2$,

$\omega = 0.8 \pm 0.3$.

Very interesting is the obtained value of the parameter *n*, which indicates that there is a single site for the specific binding of magnesium ion per two nucleobase triads.

Raman spectra corresponding to polyA without magnesium ions and to that with all the binding sites occupied by magnesium ions were then obtained by using relation (3.7). They are shown in Figure 4.10 together with their difference indicating the effect of the magnesium ion binding to the specific binding site on Raman spectrum. To interpret these spectral changes, the literature concerning RNA and Raman spectroscopy was reviewed and the main Raman markers resumed in Table 4.1.

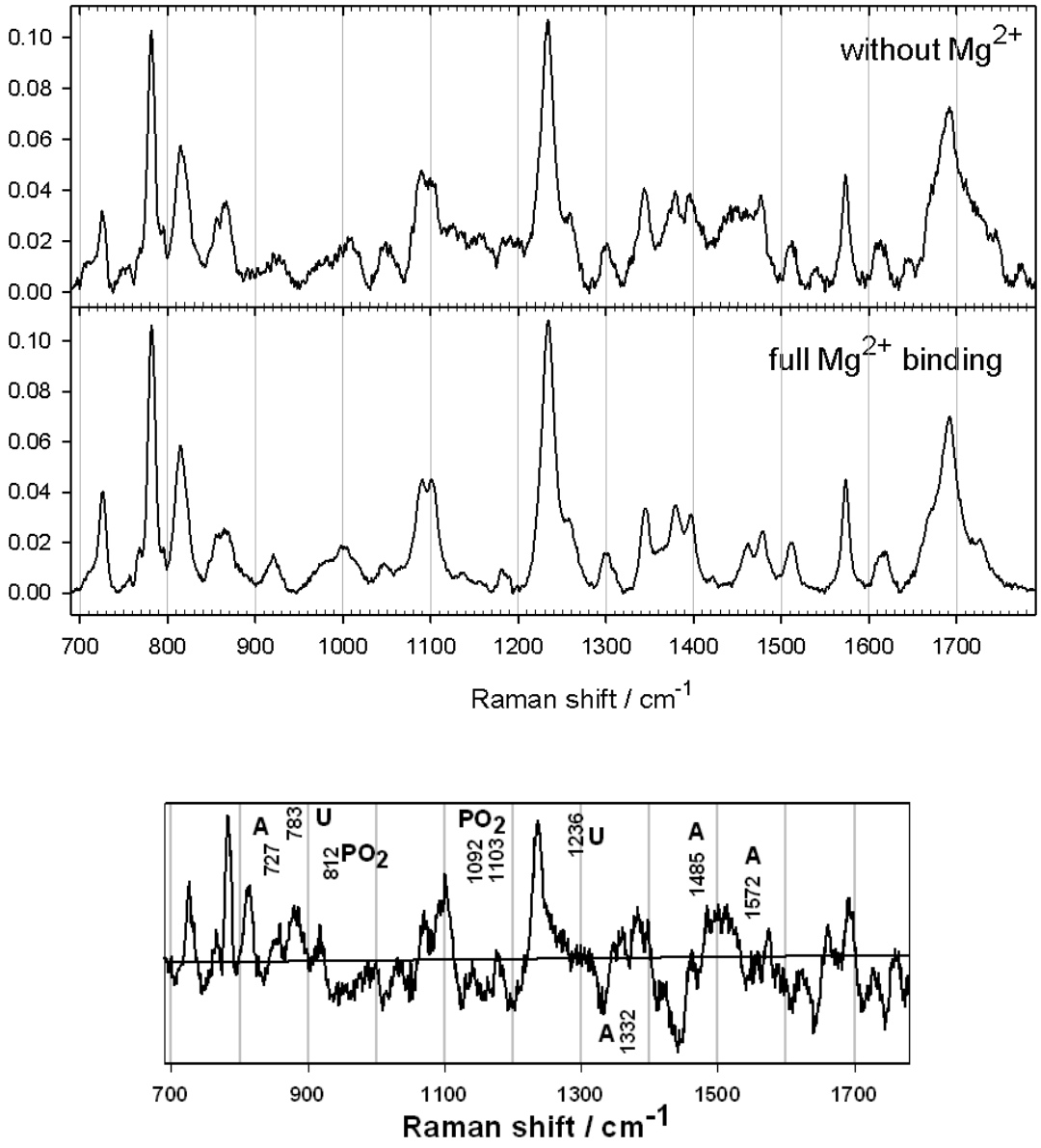

Figure 4.10. Resulting Raman spectra of polyA without and with specifically bound Mg^{2+} ions and their mutual difference (with magnesium ions minus without).

TABLE 4.1. Assignment of Raman bands present in the NA systems formed by polyU and polyA.

Band	Assignment	Refs
727	A ring breathing	[46]
783	U ring breathing	[46]
813	O-P-O stretching A RNA marker	[47,48]
881	Furanose C-O,C-C stretching	[46]
910	Furanose C-O,C-C stretching	[46]
1071	ribose stretching at 2‘	[49]
1101	PO2 sym stretching	[46,48]
1234	U ring stretching	[46, 49]
1242	U/A ring stretching	[46]
1339	A ring mode (shifted to 1347 in the triplex)	[47,46]
1347	A ring mode in 1339 in the duplex	[47]
1382	A ring mode	[46]
1450	C5’H_2 scissors	[46]
1691	U C=O stretching	[46,49]

The shape of the difference spectrum indicates that the binding of magnesium ion does not cause a strong change of any Raman band, but influences many of them. In particular, we can recognize slight intensity increase of uracil bands at 783 and 1234 cm^{-1} , adenine band at 727 cm^{-1} (together with slight upshift), and Raman band of O-P-O stretching at 813 cm^{-1}. Strong intensity decrease is also in the region of the ribose C5’H2 scissoring vibration at 1450cm^{-1} and the shape of the PO^{2-} symmetric stretch that form in triplexes a doublet is also affected.

We can conclude that in the specific binding position, Mg^{2+} is close to both adenine and uracil bases, but interacts also with the phosphate and ribose. Molecular dynamics simulations provided the most probable solution of the specific binding pocket for magnesium ion in the triplex structure inside the major-major groove (see Figure 4.11), which corresponds to the observed changes in Raman spectrum.

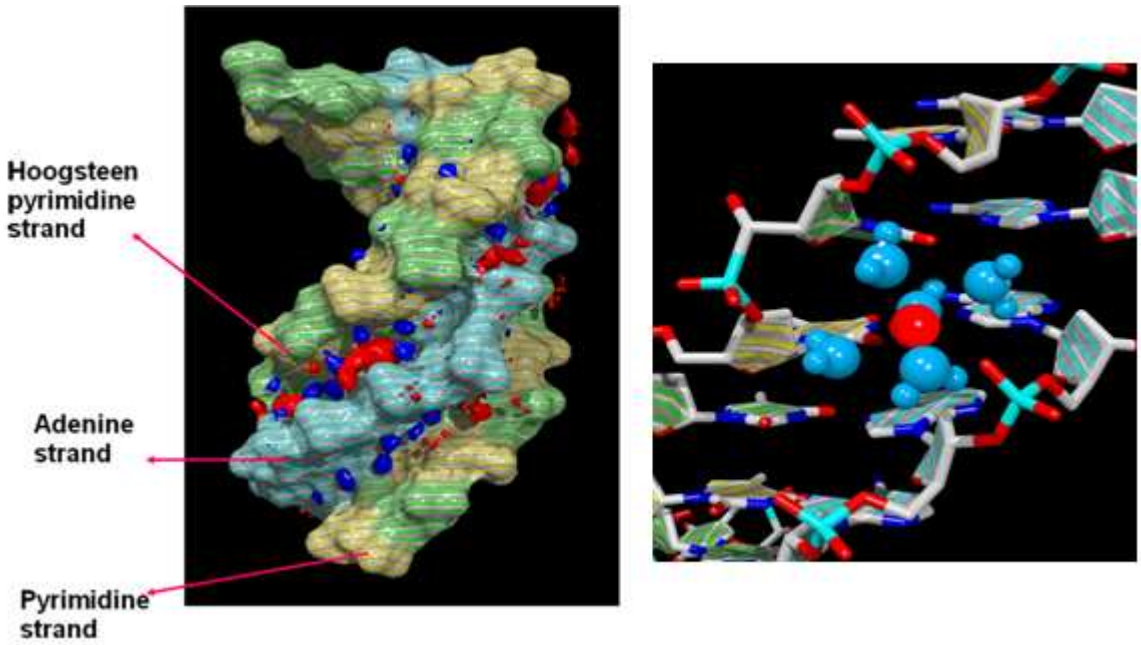

Figure 4.11. Position of the Mg^{2+} binding pocket in the polyU-polyA-polyU triplex structure (left) and the placement of solvated Mg^{2+} ion in the pocket (right) proposed on bases of Raman measurements and molecular dynamics simulation [50].

4.2 PolydA- PolydT SYSTEMS

4.2.1 Single strands of PolydA and polydT

For single strands of polydA the Raman spectra at different temperatures and with and without magnesium ions. The SVD results of the spectra without magnesium ions are shown in Figure 4.12. The singular number indicates that there are three significant spectral components; however, the third one is almost negligible. From profile of V2, it is observable a periodic change of the spectra with the increase of temperature.

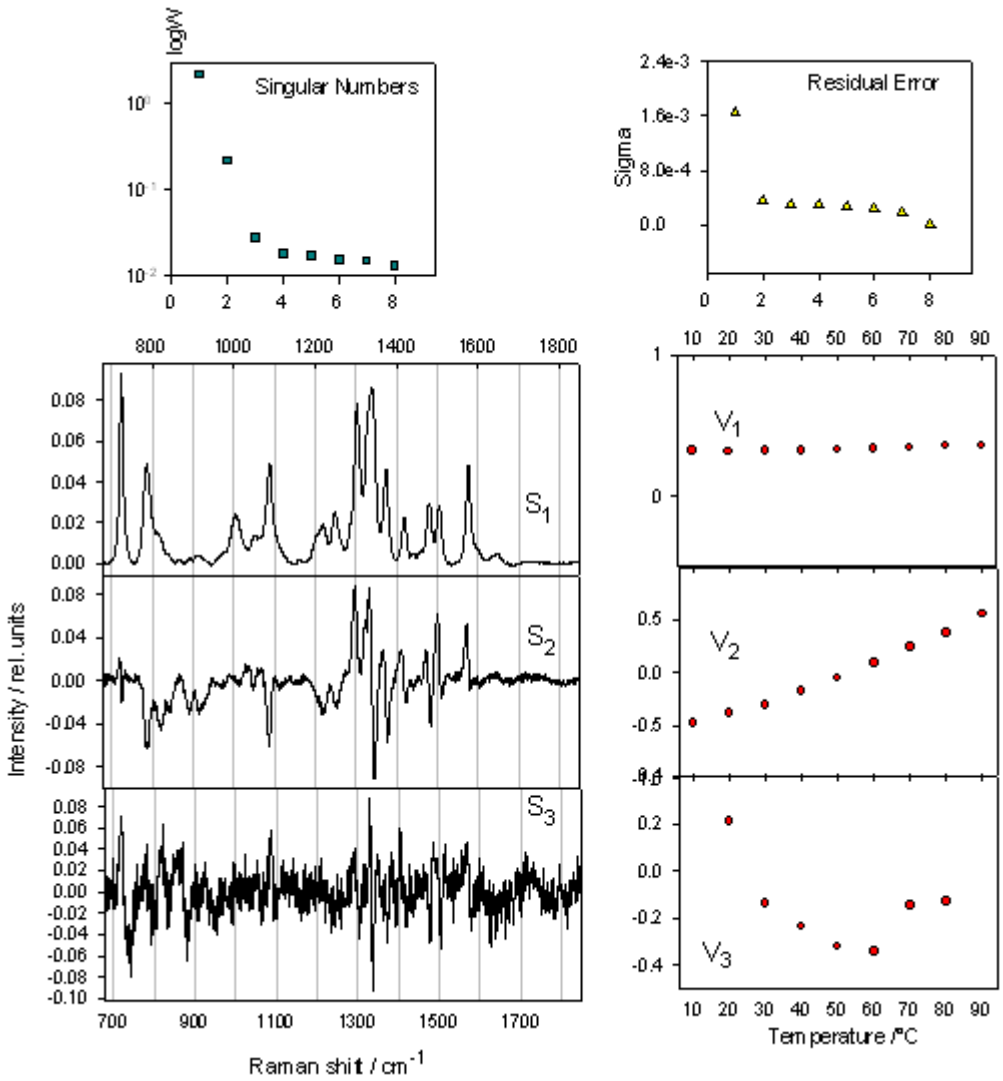

Figure 4.12. Results of the SVD analysis on polydA. Temperature changes on 20 mM polydA in 80 mM cacodylate buffer without magnesium ions.

PdA tracts in crystal structures of several oligonucleotides are seen to be straight [4], However, our experiments showed that polydA chains can not be in a straight form in solution because when the temperature increase there is a continuous change of the structure proportional to the temperature, with intensity changes of bands associated with the phosphates (1090 cm^{-1} and 790 cm^{-1}) and downshift of the Adenine band around 1500 cm^{-1} (from 1500 cm^{-1} to 1490 cm^{-1}) and the reduction of intensity of the band at 1580 associated with adenine bases.

In the case of polydT, the analysis of all the spectra measured with various concentrations of magnesium ions and with temperature changes (Figure 4.13) give only one significant spectral component. These results suggest that the structure of the polydT in solution is not affected by changes in the temperature or in the magnesium concentration.

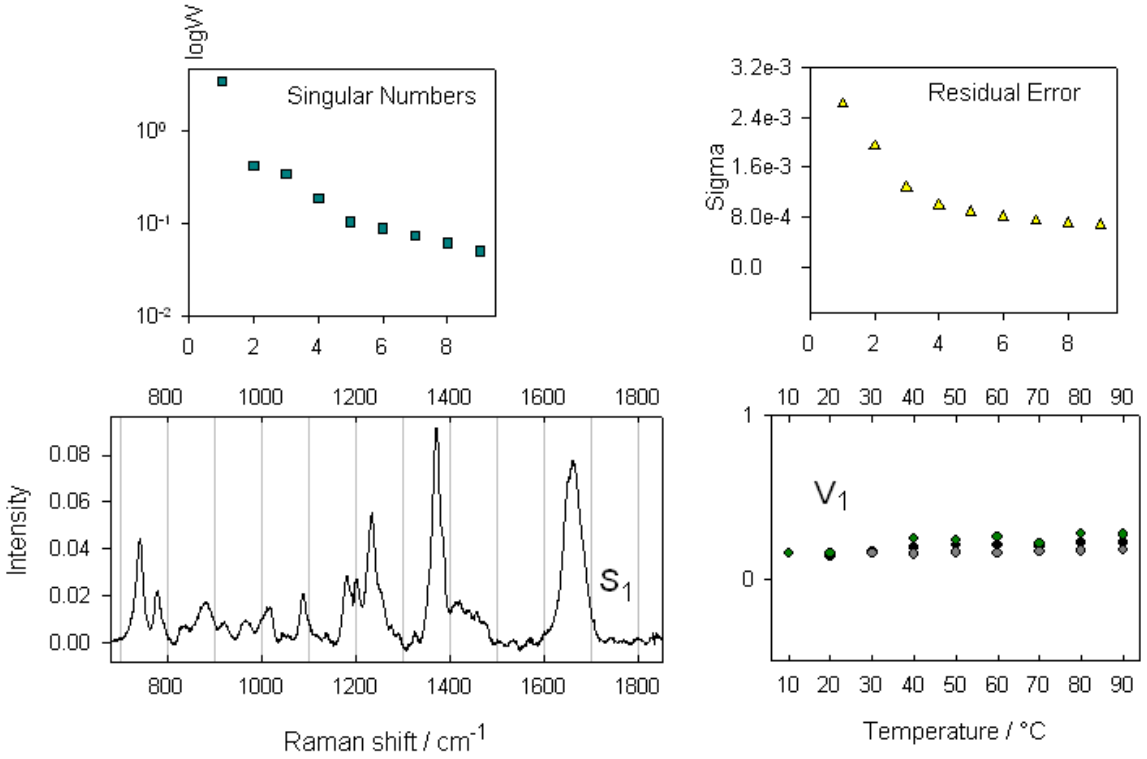

Figure 4.13. Results of the SVD analysis on polydT. Temperature changes on 20 mM polydT in 80 mM cacodylate buffer without (black), with 5 mM $MgCl_2$ (green) and with 10 mM $MgCl_2$.

4.2.2. PolydA and polydT 1:1 mixtures

Figure 4.14 shows the results of the temperature dependence of a solution of polydA and polydT with stoichiometric ratio 1:1. From the residual error and the spectral profiles of the components, we can conclude that the factor dimension of the spectral set is three.

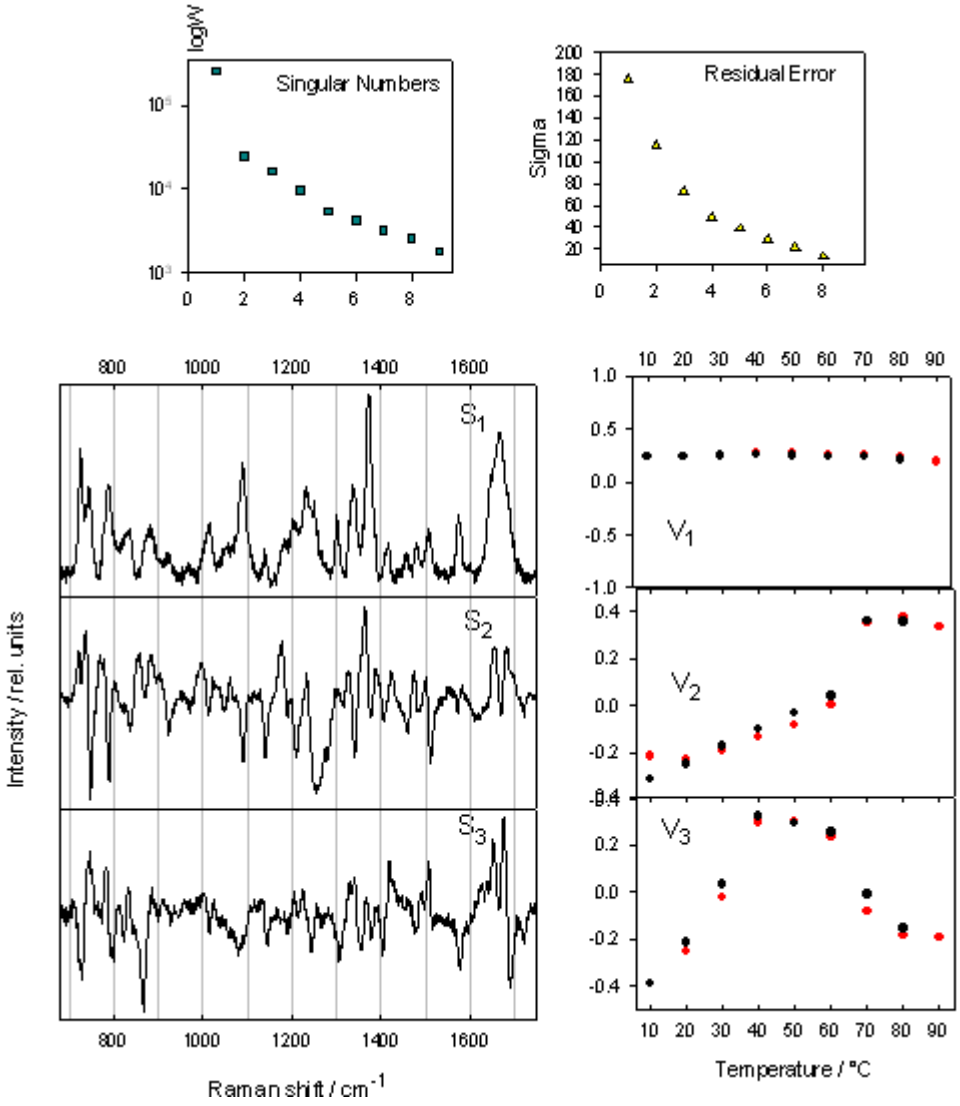

FIGURE 4.14. Results of Singular Value Decomposition applied to the Raman spectra set of 20 mM polydA-polydT in cacodylate buffer (pH 6.4) at various concentrations without magnesium ions, temperature in the range 10 – 90℃ was measured.

In the profile of the coefficients of the second component, V2, we can visualize the melting transition around 65℃. Additionally, in the profile of V3 a transition, premelting transition, in the low temperature region can be observed. This premelting transition at physiological temperatures has been subject of several studies [31, 51].

For the detailed analysis of the magnesium influence in these premelting transition we chose the spectra obtained at two particular temperatures 10℃ and 40℃, i.e.

at temperatures bellow and above the mid of the premelting transition. Figure 4.15 shows Raman spectra of polydA-polydT without magnesium ions and with 5 mM $MgCl_2$ at these two temperatures and difference Raman spectra corresponding both to the temperature effect for the same magnesium content and to the magnesium effect at the same temperature. Table 4.2 resumes the assignment of the bands and the main changes occurring during the premelting transition without magnesium according to the literature.

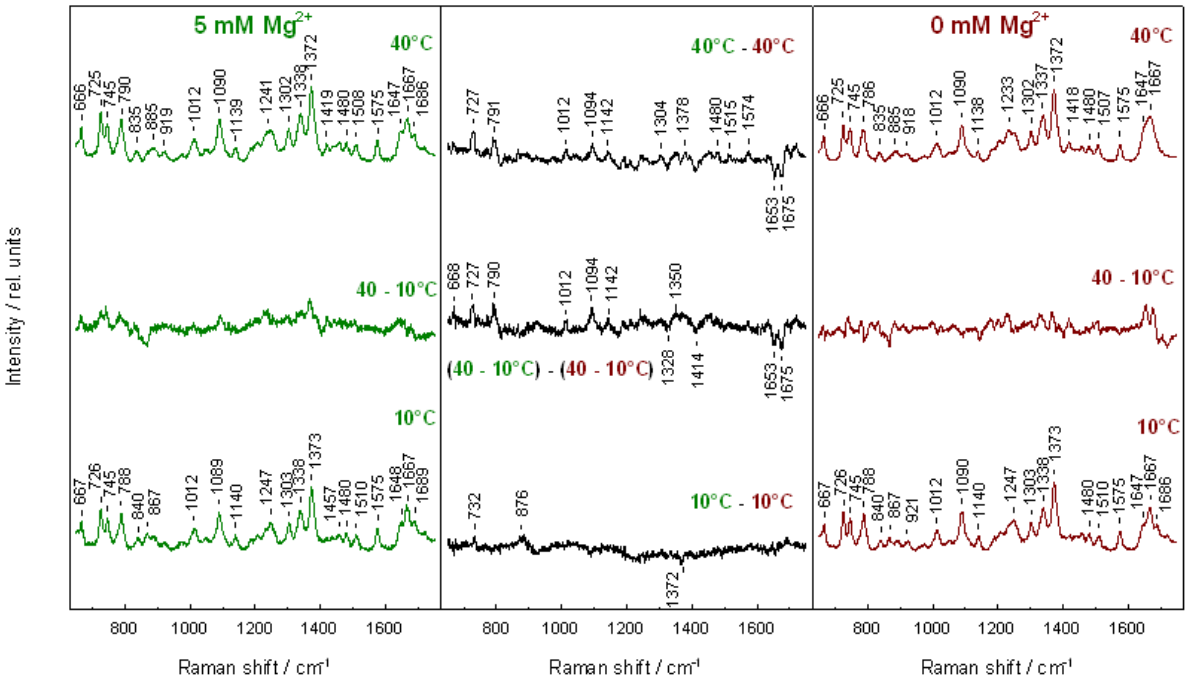

FIGURE 4.15. Raman spectra of polydA-polydT duplex at temperatures at the low and the high edge of the premelting transition, 10°C (bottom) and 40℃ (upper part) without magnesium ions (red) and with 5 mM magnesium ions (black). And their difference spectra.

The weakest difference spectrum corresponds to the polynucleotide duplex at the lower temperature (10℃) in the presence and in the absence of magnesium ions, indicating only very weak effect of magnesium binding to the duplex in B' conformation. The only resolvable peaks belong to the dA breathing vibration (732 cm-1), deoxyribose C2'H2 rocking (876 cm-1), and CH3 deformation vibration of dT (1372 cm-1). Presence of the last peak indicates that the weak binding of

magnesium to the B'-form of polydA-polydT duplex comes through the major groove of the duplex.

TABLE 4.2. Assignment of Raman bands present in the NA systems formed by polydT and polydA.

Band	Assignment	Refs
671	C2'-endo/anti thymidines	[47]
727	A ring breathing	[51]
753	C2'-endo/anti thymidines	[47, 51]
790	O-P-O stretching	[51, 48]
834	O-P-O stretching B DNA marker	[51, 48]
923	Deoxyribose ring stretching	[51]
1092	PO_2^- str	[48]
1262	A ring stretching shifts to 1243 with premelting	[51, 52]]
1378	T ring stretching shifts to 1366 with premelting	[52]
1513	A ring stretching (shifted to 1347 in the triplex?)	[47, 52, 53]
1579	A ring stretching shifts to 1571 with premelting	[52]
1661	T C=O stretching shifts to 1684 with premelting	[53]
1681	T C=O stretching shifts to 1689 with premelting	[53]

Not affected by the magnesium presence seems to be the 840-835 cm-1 downshift and the change of the thymidine 1373 cm-1 band, while Raman bands of the thymine keto-groups vibrations and the adenine band at 1510 cm-1 are changed remarkably less in the presence of magnesium.

The difference Raman spectrum of the two samples at 40℃ is of higher intensity compared with the same difference spectrum of the samples at 40℃. We can conclude that magnesium ions present stronger interaction with the B than with the B' form of the polydA-polydT duplex. The most plausible explanation is the widening of the minor groove during the transition. In the B' state, magnesium interact only weakly through the major groove, because the minor groove is too narrow. We can also observe that magnesium ions prevent the thymine moieties to reach in the B-state the same arrangement in the vicinity of their keto-groups like in the sample without magnesium.

4.3 APICAL HAIRPIN OF THE TAR SEGMENT

The studies of magnesium ion interaction with the apical hairpin-loop of the TAR segment of the genomic HIV-1 RNA follow-up previous studies accomplished in our lab. Temperature dependent Raman spectra subjected to SVD analysis revealed that besides the temperature induced melting (hairpin opening), a premelting transition occurs at lower temperatures. This transition was interpreted as a rearrangement of the nucleotides in the six-member loop [54]. Microcalorimetric measurements (DSC) confirmed existence of this transition [55] Nevertheless neither Raman spectroscopy nor DSC provides sufficiently resolved data enabling to determine thermodynamic parameters of this transition. The aim of the study accomplished within the framework of the thesis was to characterize the influence of magnesium ions on both the premelting and the melting transitions. All previous measurements were performed at 3 mM concentration of Mg^{2+}.

4.3.1. UV absorption measurements

With aim to obtain experimental data from more methods, series of precise UV absorption measurements were performed besides Raman experiments. UV absorption of three samples with 0mM, 3mM and 6 mM Mg^{2+} were measured in the temperature range from 10℃ to 90℃. Figure 4.16 sh ows as an example the series of UV spectra obtained for the sample without magnesium. At the first sight the temperature effect seems to influence only the high of the long-wavelength absorption band. In fact there are also subtle changes of the spectral shape that can be revealed by means of factor analysis.

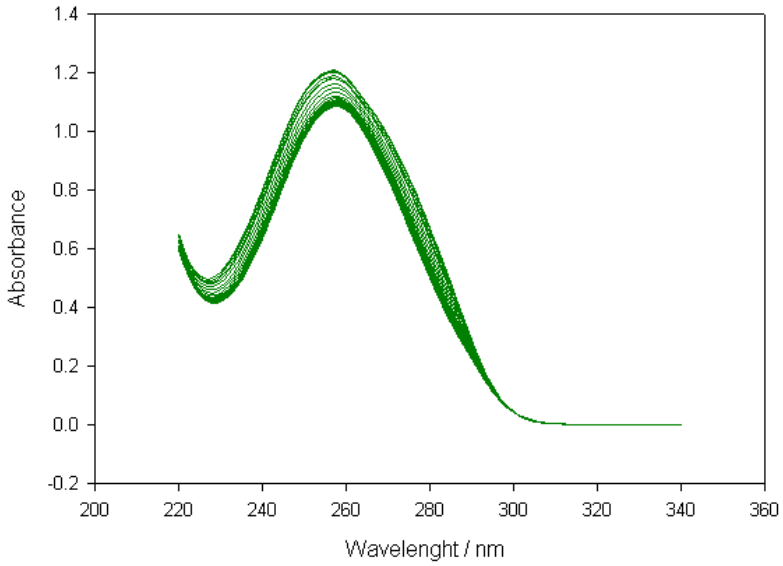

FIGURE 4.16. Set of UV absorption spectra obtained for 7.5 µM per oligonucleotide of solution of TAR 14-mer oligonucleotide without magnesium. The curves correspond from the lower to the upper to temperatures from 10℃ to 90℃.

Figure 4.17 shows results of a common SVD applied to catenated the three spectral series. The respective temperatures are given by the x-axis of the coefficients plots and the concentrations of magnesium ions by the symbol colors. The factor dimension of the spectral set is obviously four. The coefficients plots for all four spectral components display the dominance of the temperature effect over the effect of magnesium ions concentration. The plots of the coefficients V_1 and V_2 clearly show the melting transition with the temperature of the hairpin opening around 70℃. The third and the forth components des cribe mainly the spectral changes in the premelting temperature region. While V_3 exhibits smooth curve without any sign of the transition temperature, the sigmoidal shape of V_4 shows a premelting transition around 37℃ (for the samples with magnesium).)

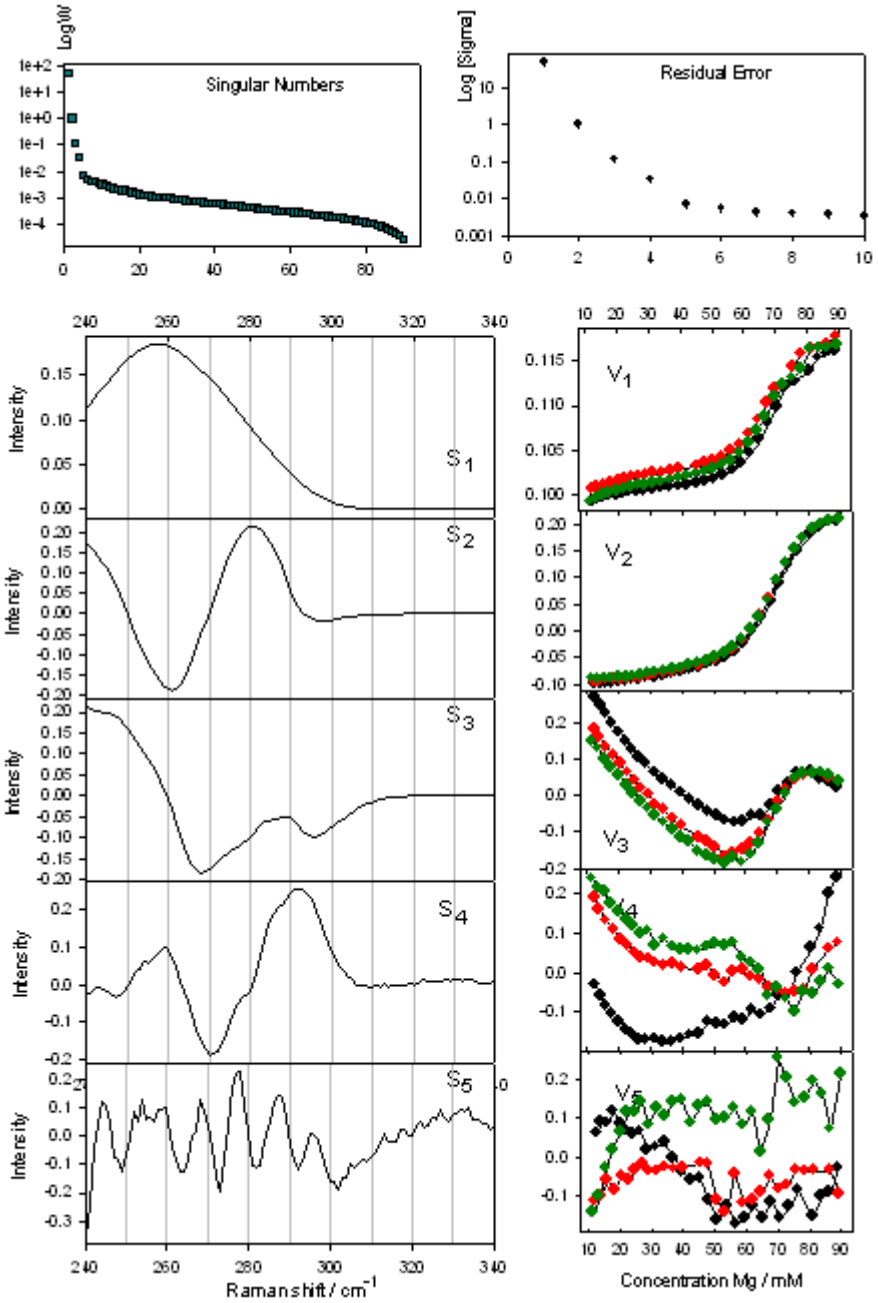

FIGURE 4.17. Results of the SVD analysis of UV absorption spectra. Temperature changes on TAR solution with a concentration of 7,5 µM per nucleotide in 20 mM cacodylate buffer containing 140 mM KCl and 20 mM NaCl. $MgCl_2$ concentrations are 0 mM magnesium (in black), for the sample with 3 mM magnesium (red) and for the samples with 6 mM magnesium (green).

The concentration of magnesium ions seems to influence mainly the premelting transition, because the V_2 curves seem to be almost identical for all samples in the melting region. (The differences between V_1 curves for particular Mg^{2+}

concentrations correspond rather to slight alterations of the oligonucleotide concentrations than to the magnesium effect.)

The temperature dependences of V1, V2, V3, and V4 coefficients were fitted according to a model considering two monomolecular transitions. The least square fit was performed simultaneously for the four coefficients, but independently for particular concentrations of magnesium ions. Results of the fit are described in Figure 4.18. as solid lines in the plots of the coefficients. The obtained thermodynamic characteristics of both transitions are presented in Table 4.3.

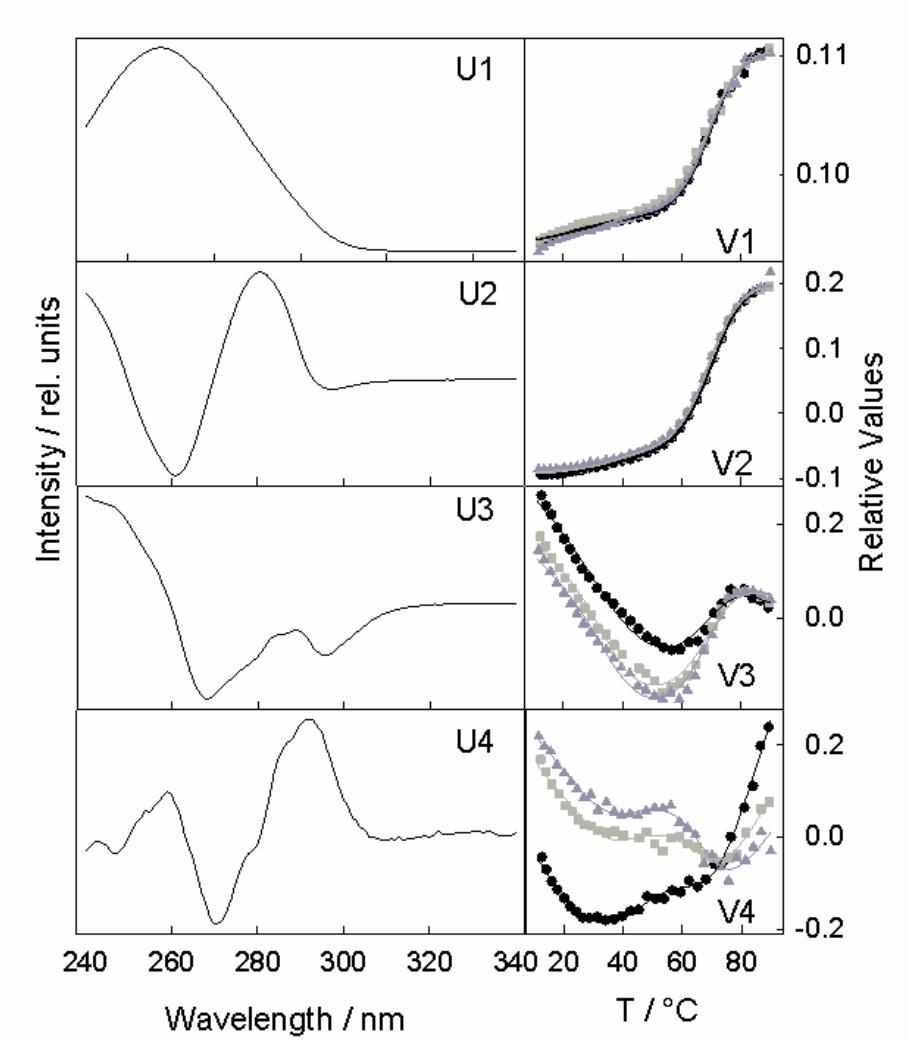

FIGURE 4.18. Results of SVD analysis of UV absorption spectra (as in Figure 4.12) with the fitted temperature dependences of the V1 – V4 coefficients (solid lines).

TABLE 4.3. Calculated thermodynamic parameters from measurements of UV absorption for the TAR 14-mer at various magnesium concentrations.

	premelting				melting			
Mg^{2+} conc. mM	T_m °C	ΔH kcal/ mol	ΔS cal/ (mol K)	$\Delta G°_{10°C}$ kcal /mol	T_m °C	ΔH kcal/ mol	ΔS cal/ (mol K)	$\Delta G°_{37°C}$ kcal/ mol
0	41 ± 2	-22.5	-72	-2.1	72 ± 1	-39.1	-113	-4.0
3	38 ± 2	-34.5	-111	-3.0	70 ± 1	-39.8	-116	-3.9
6	37 ± 1	-37.8	-101	-2.8	71 ± 1	-41.7	-122	-4.0

Considering the well known fact that the values of the enthalpy and entropy changes obtained from a fit are not very precise because of they correlated effect on the sum of the squared deviations, we should compare mainly the transition temperatures and the changes of the Gibbs energy. From these quantities we can conclude that the temperature induced TAR hairpin opening is practically not sensitive to magnesium, but magnesium ions affect the transition in the low-temperature region.

The fit also provides estimated percentages of the three forms of the hairpin, the "low-temperature" closed form, the "high-temperature" closed form and the open form, shown in Figure 4.19. The Figure, as well as Table 4.3, clearly demonstrates that the magnesium presence influences mainly the premelting transition, which is in the presence of magnesium sharper and shifted to lower temperatures. The 3 mM concentration of magnesium ions is sufficient to induce this effect and further increase of magnesium ions changes the transitions only marginally.

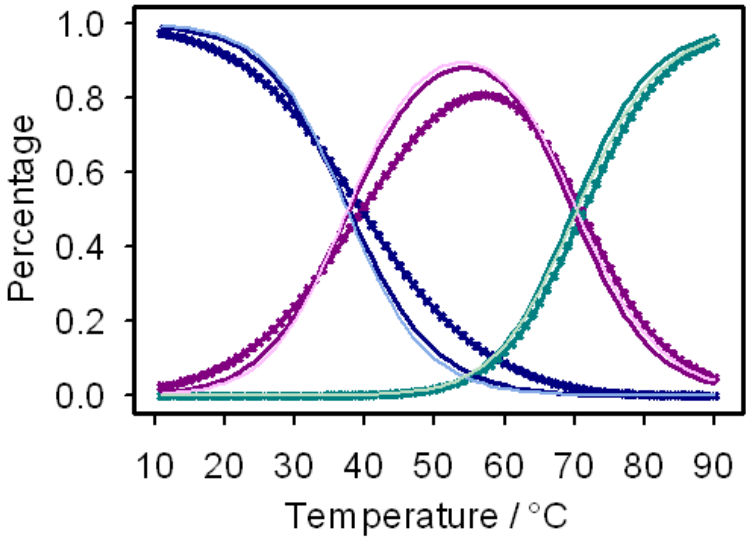

FIGURE 4.19. Temperature dependence of the three forms of loops occurrence (percentage) calculated with the results of the fit of the coefficients; blue: closed form 1, red: closed form 2, green: open form of the hairpin; smooth curves corresponding to samples with $MgCl_2$: dark colors 3 mM and light colors 6 mM $MgCl_2$.

4.3.2. Raman measurements

Raman spectra were measured for the sample with 6 mM concentration of magnesium ions and that without magnesium in the temperature range of 10 – 85℃ with 5℃ temperature steps. The obtained sets of background-corrected Raman spectra are shown in Figures 4.20 and 4.21 as the Raman spectrum at 10℃ and differences of the spectra obtained for hi gher temperatures in respect to the low-temperature spectrum. The spectral region between 897 and 1060 cm-1 was cut off because of some bands belonging to low-molecular impurities (inorganic phosphates).

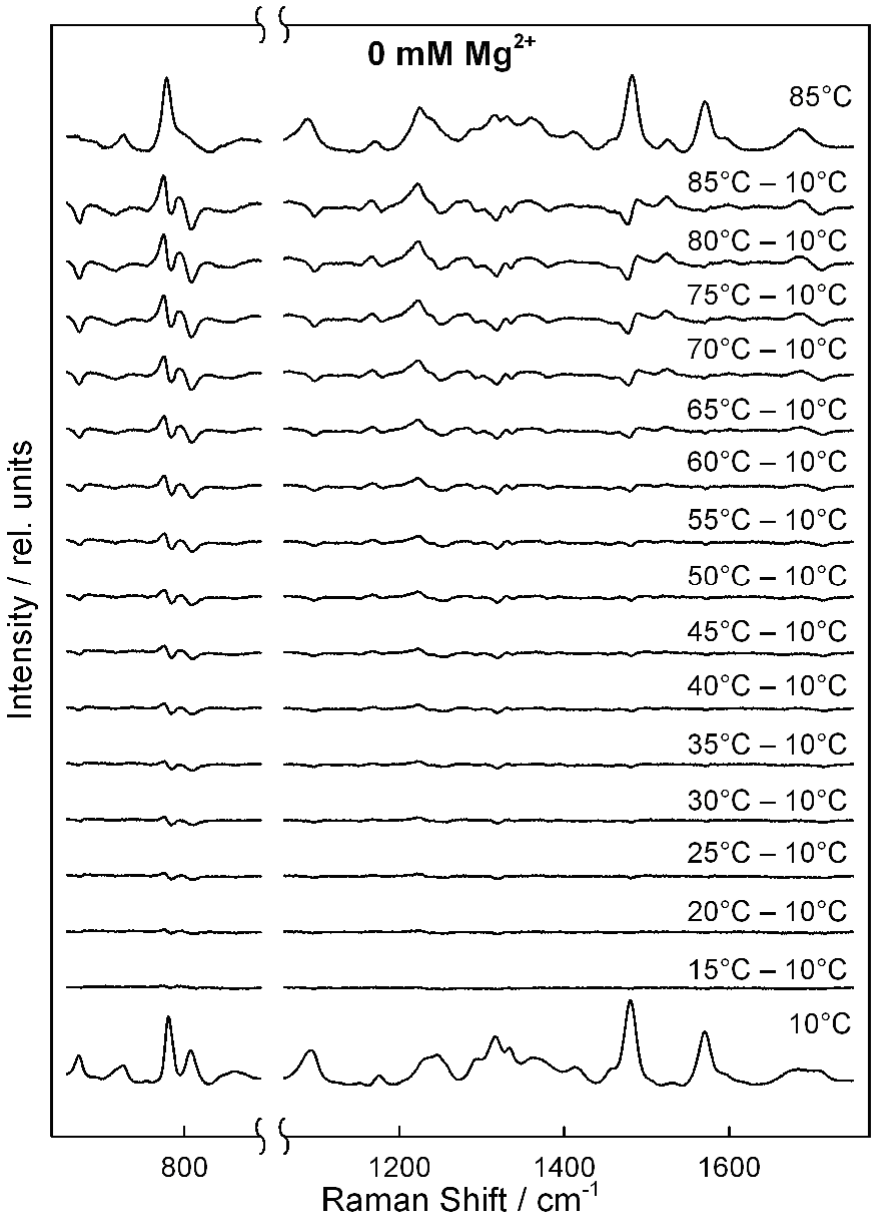

FIGURE 4.20. Raman spectra of 1.4 mM TAR hairpin in solution without magnesium ions (20 mM sodium cacodylate buffer containing 140 mM KCl and 20 mM NaCl), pH 6.4, at 10℃ (bottom). The other curves represent the difference spectra at the indicated higher temperature minus the 10℃ spectrum.

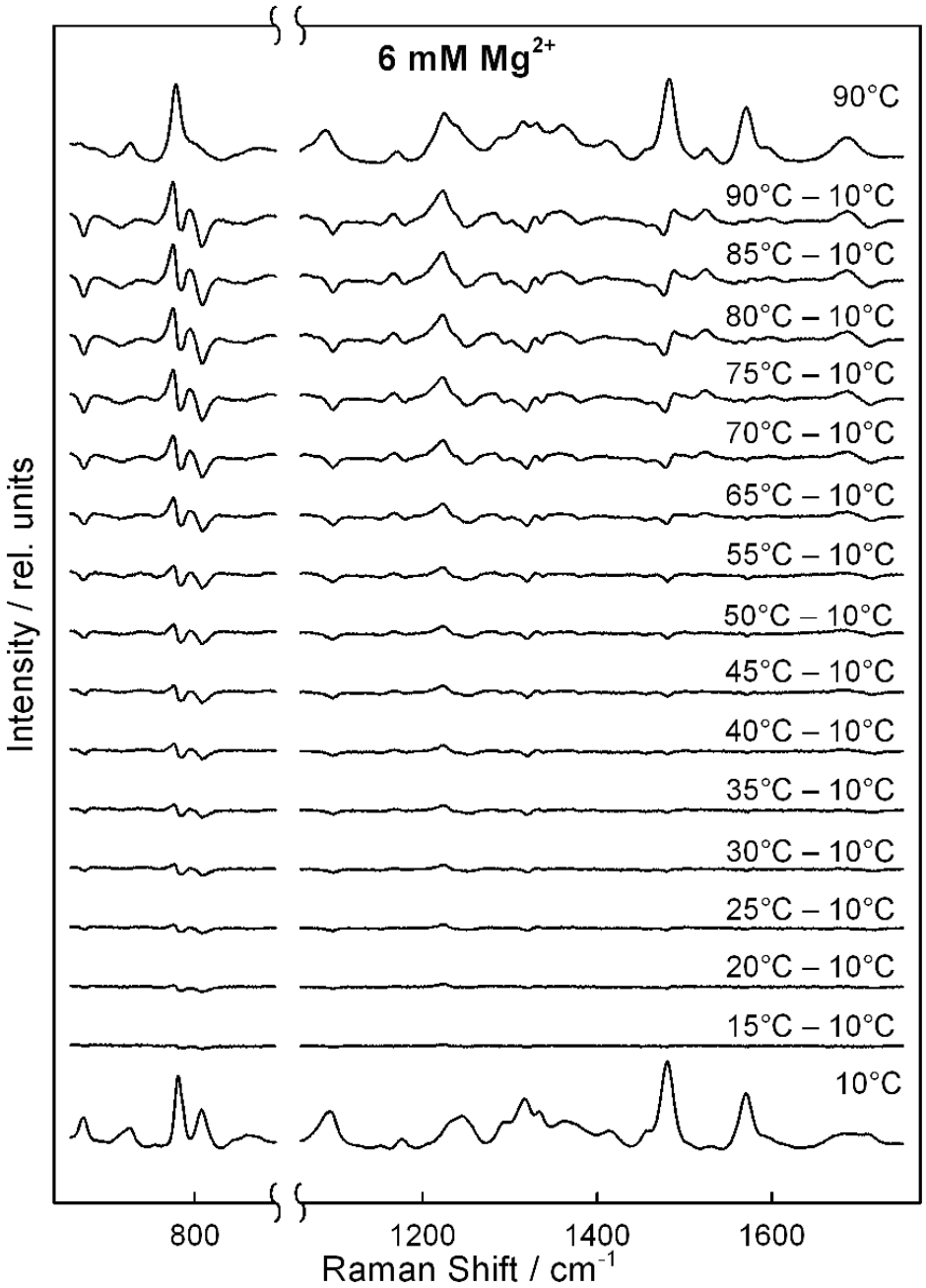

FIGURE 4.21. Raman spectra of 1.4 mM TAR hairpin in solution with 6 mM magnesium ions (20 mM sodium cacodylate buffer containing 6 mM $MgCl_2$, 140 mM KCl and 20 mM NaCl), pH 6.4, at 10℃ (bott om). The other curves represent the difference spectra at the indicated higher temperature minus the 10℃ spectrum.

For the further analysis, the data measured under both conditions, without and with 6 mM $MgCl_2$, were together subjected to factor analysis (SVD). The results are shown in Fig 4.22. Comparing SVD results of Raman spectra with those of UV

absorption (Figure 4.17), we can conclude that both methods display the effects of the temperature and of the magnesium presence coherently. The main difference is that due to a lower signal-to-noise ratio, Raman spectra provide only three reliable spectral components.

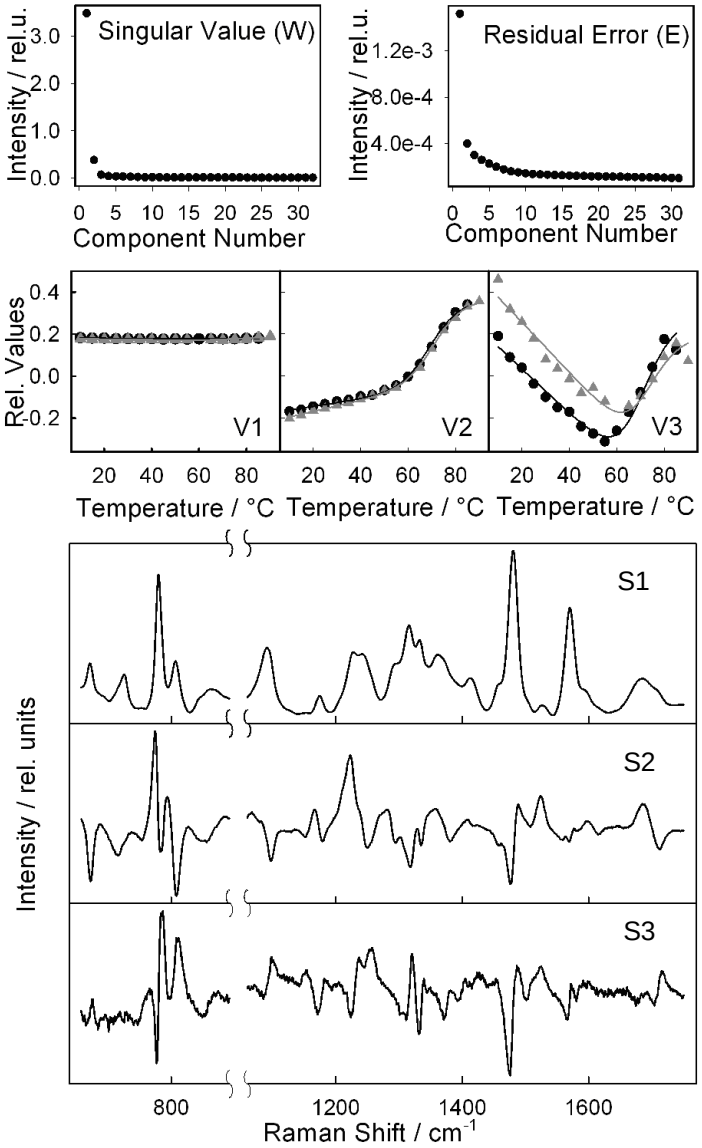

FIGURE 4.22. Results of the SVD analysis of Raman spectra. Temperature changes on TAR solution with a concentration of 1.4 mM per nucleotide in 20 mM cacodylate buffer containing 140 mM KCl and 20 mM NaCl. $MgCl_2$ concentrations are 0 mM magnesium (in black) and for the samples with 6 mM magnesium (gray).

Due to this reduction of the factor dimension, there is missing the spectral component exhibiting visible sigmoid profile in the region of premelting (like the fourth component in the case of UV absorption). This is why the Raman data themselves do not allow the determination of thermodynamic characteristics for the premelting transition. In [54] the temperature induced changes in the temperature range below the melting were modeled as a linear change of Raman spectrum with temperature. As the first attempt on a quantitative analysis of Raman data we fitted the same model to both sets of Raman spectra. The fitted temperature dependences of the coefficients V1, V2 and V3 are shown as solid lines in Figure 4.22. They agree with the experimental data very well.

The fit provided percentages of the closed and the open forms of the hairpin at various conditions (see Figure 4.23) and "pure" Raman spectra corresponding to particular hairpin forms. By using the model with linearly temperature dependent spectrum in the premelting region, we can obtain the spectrum of the open hairpin, the spectrum of the closed hairpin at the melting temperature and the spectrum of the closed hairpin at a substantially lower temperature. These spectra with their mutual differences are shown in Figures 4.24 and 4.25.

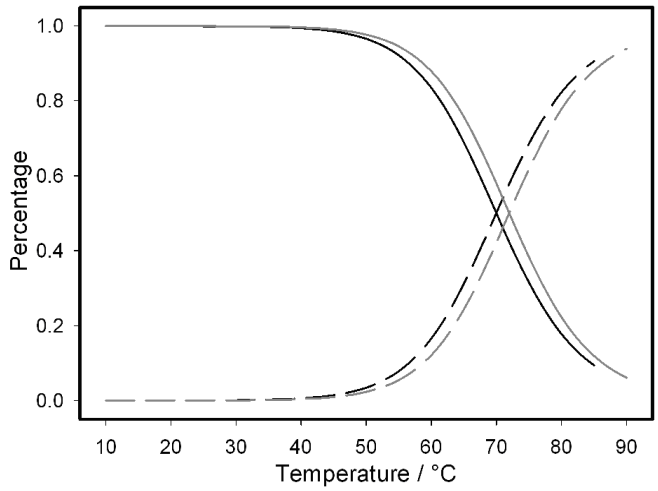

FIGURE 4.23. Temperature dependence of the closed and open forms of loops occurrence (percentage) calculated with the results of the fit of the coefficients of Figure 4.22. Solid line: closed form 1, dash line: open form of the hairpin.

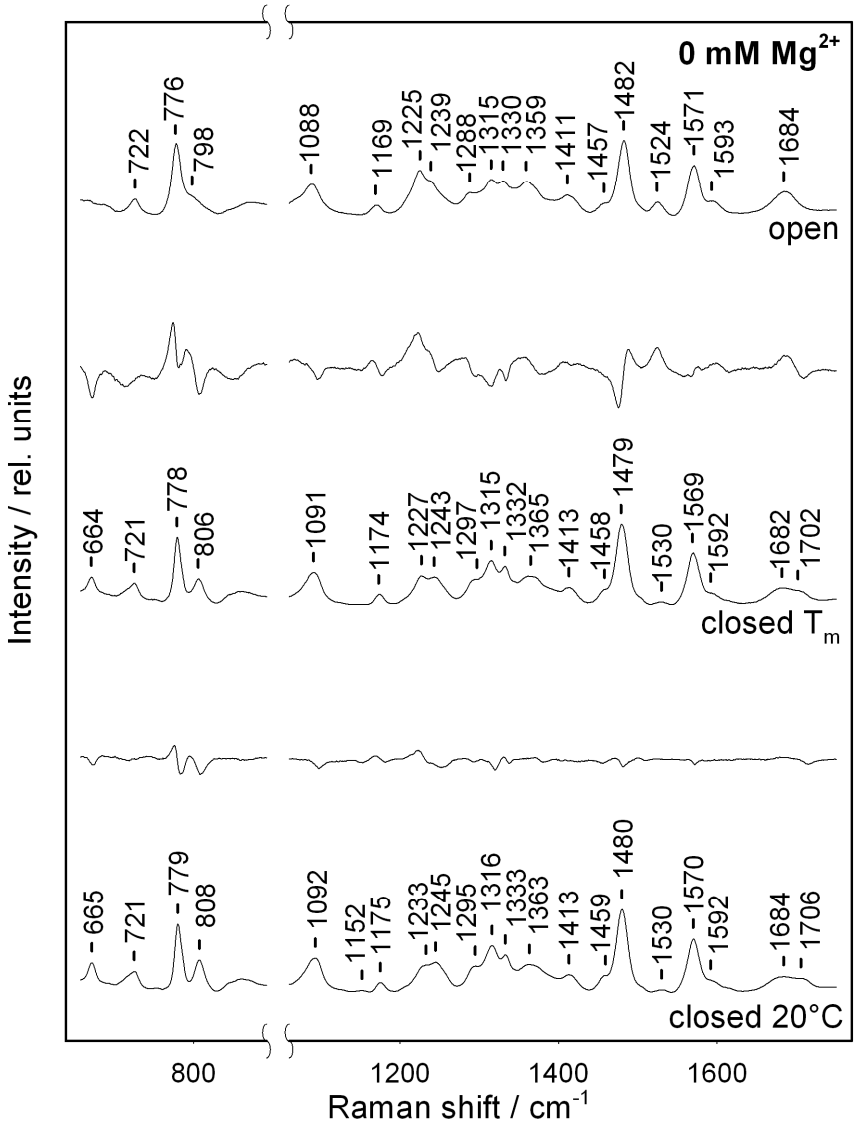

FIGURE 4.24. Raman spectra of the closed TAR hairpin without magnesium at temperatures of 20℃ and T_m, 70℃, and the spectrum of the open form at T_m, 70℃. The difference spectra are shown in between .

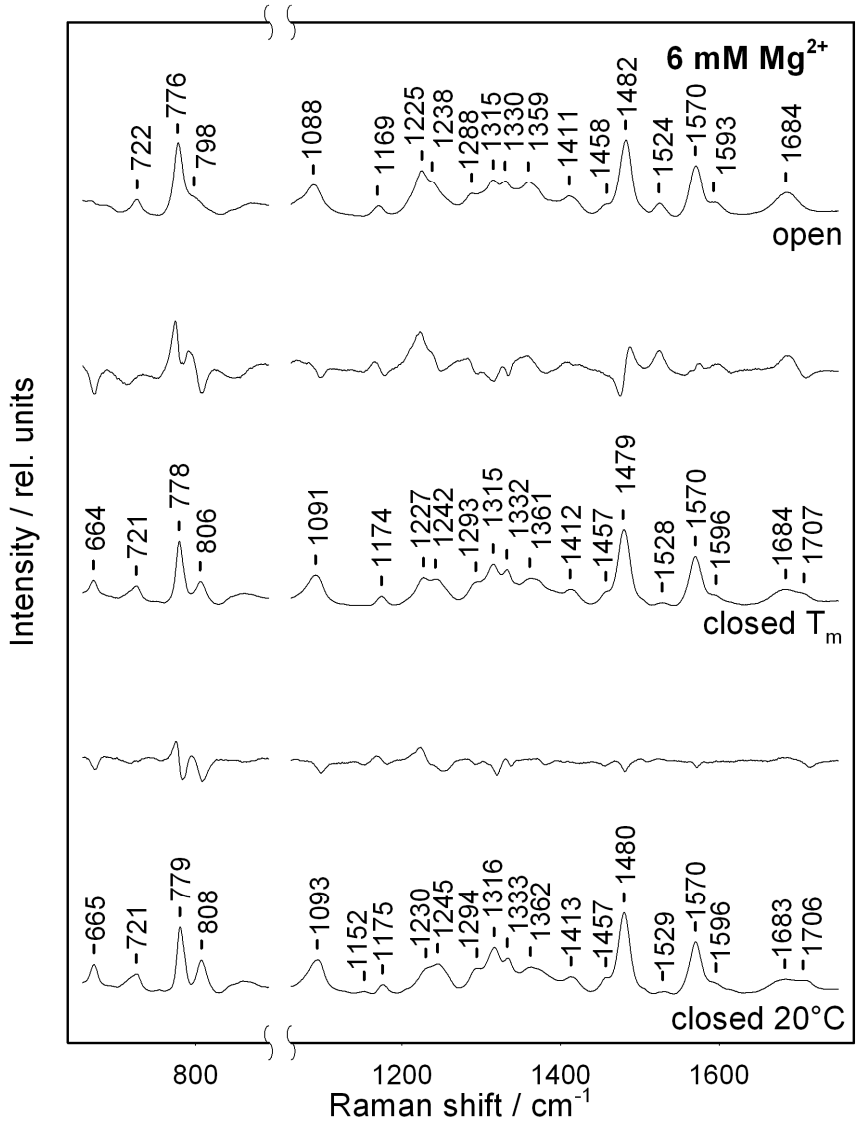

FIGURE 4.25. Raman spectra of the closed TAR hairpin with 6 mM concentration of magnesium ions at temperatures of 20℃ and T_m, 70℃, and the spectrum of the open form at T_m, 70℃. The difference spectra are shown in between.

Second variant of Raman data analysis was a fit according to the full model considering both the melting and the premelting transition. The thermodynamic parameters of the premelting transition were though taken from the UV experiment (Table 4.3). The results of the fit are shown in Figure 4.26.

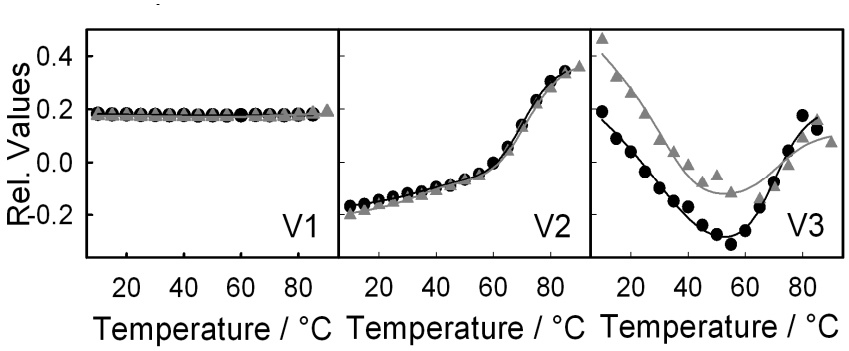

FIGURE 4.26. The SVD coefficients from factor analysis of Raman spectra (as in Figure 4.18) with the fitted their temperature dependences by the model considering two transitions – parameters of the premelting transition taken from the results of UV absorption measurement (solid lines). Without (black) and with 6 mM (gray) magnesium ions.

The fit to the full model provides also the percentages of individual forms. The results are shown in Figure 4.27. In the temperature region where only two forms of closed hairpins coexist, the plot is equivalent to that obtained from UV measurement (Figure 4.19). It is a direct consequence of the use of the thermodynamic parameters from UV measurement. The occurrence of the open hairpin is, on the other hand, the same as in Figure 4.23.

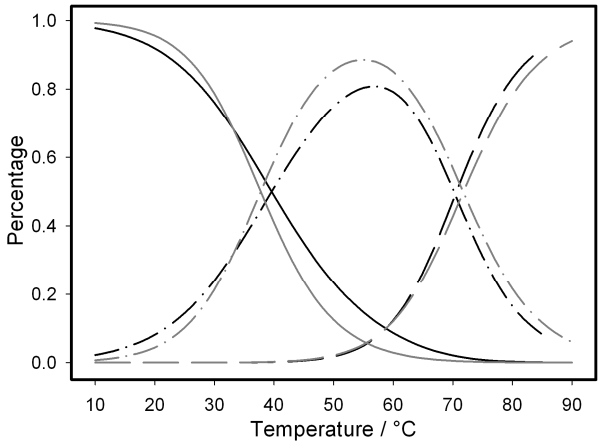

FIGURE 4.27. Temperature dependence of the three forms of loops occurrence (percentage) calculated from the results of the fit of the SVD coefficients (SVD of Raman spectra, fit of the full model – see the text). Solid line: closed form 1, dash-dot line: closed form 2, dash line: open form of the hairpin. Without (black) and 6 mM (gray) magnesium ions.

Raman spectra constructed for the two closed hairpin forms and for the open form on the basis of the full model fit were not distinguishable from those in Figures 4.24 and 4.25.

To visualize the magnesium-ion effect on the premelting transition, we can plot mutual differences between Raman spectra obtained at two distinct temperatures above and bellow the midpoint of the premelting transition and for the samples with and without magnesium ions (Figure 4.28).

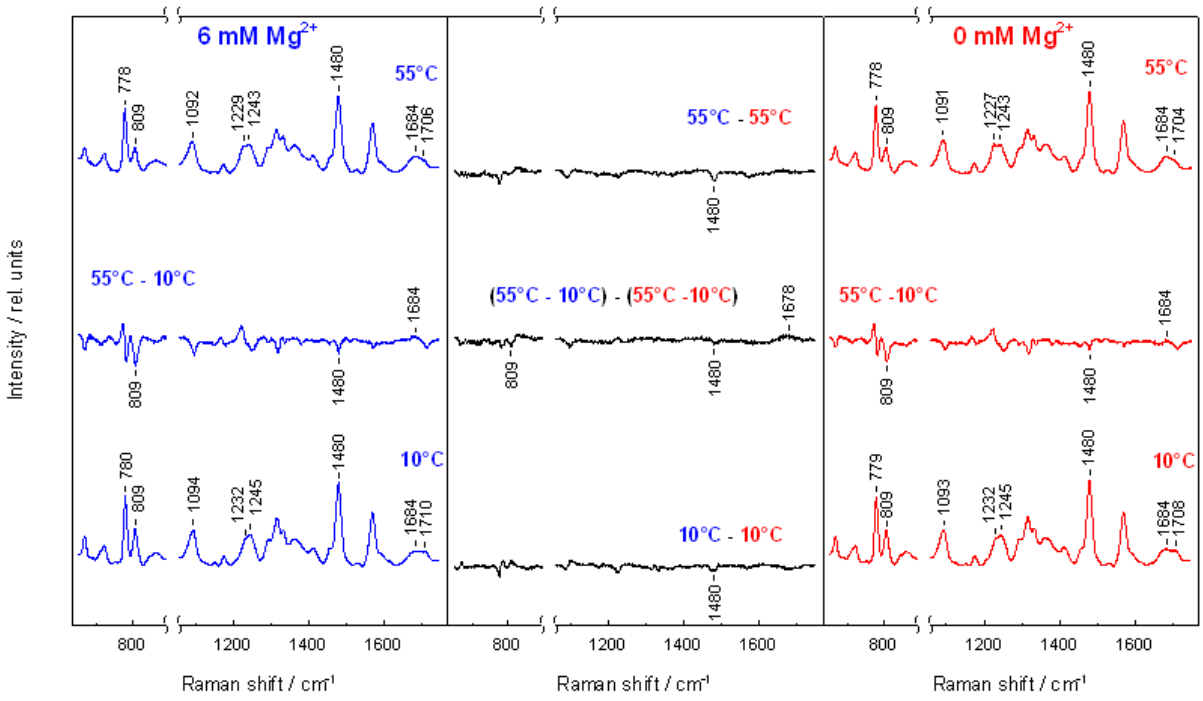

FIGURE 4.28. Raman spectra of apical TAR hairpin at temperatures at the low and the high edge of the premelting transition, 10℃ (b ottom) and 55℃ (upper part) without magnesium ions (red) and with 6 mM magnesium ions (blue). And their difference. For a better visibility, all difference spectra are multiplied by a factor of two.

At the first sight, the magnesium effect expressed by relevant difference spectra is clearly observable in the case of TAR premelting transition, but it is substantially weaker than, e.g., in the case of the premelting transition observed for polydA-

polydT duplexes. We can see that the changes of Raman spectra measured at the same temperature but with or without magnesium ions are for many Raman bands analogous to those caused by the temperature increase. This means that the basic tendency in the difference spectra is the support of the premelting transition by magnesium ions.

The assignment of the Raman bands observed in these spectra are resumed in Table 4.4, where we also show the effect of magnesium in each of the different forms of the hairpin, the closed forms at 20℃ and Tm (70℃), and the open form at Tm. The weak but resolvable effects of magnesium ions involve numerous Raman bands, but as a rule there is always change on Raman bands of C=O stretching (guanine and uracil) at 1682 and 1702 cm^{-1}, the ring vibration of guanine at 1480 cm^{-1}, and the breathing vibration of uracil at 780 cm^{-1}. This indicates that keto-groups of the unpaired nucleobases in the loop represent preference sites for, maybe only temporal, binding of solvated magnesium ions.

We can conclude that our study of the magnesium influence on solutions of the apical TAR hairpin by the two methods, UV absorption and Raman spectroscopy, shows that the premelting transition is influenced weakly but still measurably by magnesium ions. The main effect of magnesium ions is the support of the structural changes in favor of the arrangement reached at the temperature above the premelting, due to an unspecific improvement of the electrostatic shielding, but there are also signs of magnesium interactions with nucleobases in the loop via their keto-groups.

TABLE 4.4. Raman bands present in the TAR 14-mer Raman spectra and the effect of magnesium ions.

Band* cm^{-1}, int.**	**Assignment**	**Closed** 20°C	**Closed** T_m	**Open** T_m	**Refs**
664	C, A	→			[46,49]
721	A ring breathing				[46]
778	C+U ring breathing	⇓	⇓	⇓	[46]
806	O-P-O stretching A RNA marker	⇓			[47,48]
1091	PO2 sym stretching	→	⇓		[46,48]
1174	G 3'-endo/syn			←	[57,58]
1227	U ring stretching	←⇓		←	[46,49]
1243	U,C,A ring stretching			←	[46]
1297	C 3'-endo/anti	←	←		[59]
1315	G 3'-endo/anti	→			[60]
1332	A ring mode				[46,47]
1365	G	→			[47]
1413	G				[58,59,60]
1458	C5'H_2 scissors	←			[46]
1479	G	⇓	⇓	⇓	[58, 60]
1530	C, hypochromic		←		[58]
1592	C	→	→⇓	→⇓	[58, 60]
1682	U C=O stretching	←⇓	←	→	[46,49]
1702	U,G C=O stretching	⇓	→		[58,59]

Changes of Raman bands intensities (⇓,) and positions (←,→) caused by the presence of magnesium ions.

* Parameters for the bands in the spectrum of the closed hairpin at the melting temperature in the sample without magnesium.

5. CONCLUSIONS

The investigations of magnesium ions interactions with chosen nucleic-acid molecular models, performed mainly by using Raman spectroscopy followed by factor analysis of spectral series and/or calculation of difference Raman spectra, have revealed that magnesium ions affect nucleic acids very differently, depending on the particular structural arrangement, the kind of the nucleic acid, the nucleobase composition, etc.

In the case of polyA and polyU mixed solutions, behavior of magnesium ions is driven by the existence of an energetically favorable, specific binding site in the polyU-polyA-polyU triplex structure. We have confirmed via Raman spectroscopy that magnesium ions added to a solution of polyA-polyU duplexes force some of them to dissociate and to form triplex structures. By means of magnesium-ion Raman titration we obtained Raman signature of the specific binding site, which was then localized in the major-major groove between the adenyl and the Hoogsteen uridyl chain. Application of McGhee-von Hippel model has revealed that magnesium ions can bind to this specific site every other nucleobase triad.

Magnesium ions influence not only the melting transitions or the duplex-triplex equilibrium, but they measurably influence more subtle premelting transitions, which was demonstrated on two model systems, polydA-polydT duplex and apical TAR hairpin. However, the magnesium ions affect them in quite different ways. In the case of polydA-polydT duplex, magnesium effect is much stronger and concerns mainly the stabilization of the low temperature conformation. Some spectral changes attributable to geometry changes of the structural form above the premelting transition were though also observed and it was shown that they are related to the binding of solvated magnesium ion to the minor groove after its widening as a result of the premelting transition. In the case of the apical TAR hairpin, the premelting transition is influenced relatively weakly but still clearly. The

main effect of magnesium ions is the support of the structural changes in favor of the arrangement reached at the temperature above the premelting.

6. REFERENCES

[1] Saenger W.: Principles of nucleic acid structure, Springer-Verlag, ISBN 3-540-90761-0, New York, 1984.

[2] Bloomfield V. A.; Crothers D. M.; Tinoco I., Jr.: Nucleic acids: structures, properties and functions, University Science Books, Sausalito, California, 2000.

[3] Watson J.D. and Crick F.H.C., Molecular structure for nucleic acids: a structure for deoxyribose nucleic acid. Nature, 171 (1953), 737–738.

[4] Egli M. Nucleic acids in chemistry and biology. Blackburn G.M, Gait M.J., Loakes J.D. and Williams D.M., Eds. 3rd edition. Royal Society of Chemistry. Cambridge, UK, 2006, 13-75. (and citations therein)

[5] Keene F.R., Smith J.A., and Colins J.G., 2009. Metal complexes as structure-selective binding agents for nucleic acids. Coordination Chemistry Reviews 253 (2009) 2002-2035.

[6] Voet D., Voet J. Biochemistry. 2nd edition. J. Wiley & Sons. New York, 1361.

[7] Bansal M. DNA structure: revisiting the Watson-Crick double helix. Current Science. 85 (11) (2003), 1556-1563.

[8] Seeman N.C. DNA in a material world. Nature 406 (6796) (2000), 605-608.

[9] Varani G. Exceptionally stable nucleic acid hairpins. Annu. Rev. Biophys. Struct. 24 (1995), 379-404.

[10] Rosu F., GAbelica V., Houssier C. Colson P. and De Pauw E. Triplex and quadruplex DNA structures studied by electrospray mass spectrometry. Rapid Commun. Mass Spectrom. 16 (2002), 1729-1736.

[11] Seidman M.M. and Glazer P.M. The potential for gene repair via triple helix formation. J. Clin. Invest. 112 (2003), 487-494.

[12] Chirila T.V., Rakovczy P.E., Garrett K.L., Lou X. and Constable I.J. The use of synthetic polymers for delivery of therapeutic antisense oligodeoxynucleotides. Biomaterials. 23 (2002), 321-342.

[13] Otto C., Thomas G.A., Rippe K., Jovin T.M. and Peticolas W.L. The hydrogen-bonding structure in parallel-stranded duplex DNA is reverse Watson-Crick. Biochemistry 30 1991), 3062-3069.

[14] Bindewal E., Hayes R., Yingling Y.G., Kasprzak W., and Shapiro B.A. RNA Junction: a database of the RNA junctions and kissing loops for three-dimensional structural analysis and nanodesign. NAR 83 (2008), 392-397.

[15] Chang K.-Y. and Tinoco I., Jr. Characterization of a "kissing" hairpin complex derived from the human immunodeficiency virus genome. Proc. Natl. Acad. Sci. 91 (1994), 8705-8709.

[16] Hud N.V. and Polak Matjaz. DNA–cation interactions: the major and minor grooves are flexible ionophores. Current opinion in structural biology. 11 (2001), 293-301.

[17] Anastassopoulou. Metal – DNA interactions. Journal of Molecular Structure. 651-653 (2003), 19-26.

[18] Kaim W. and Schwederski B. Bioinorganic chemistry: inorganic elements in the chemistry of life, an introduction and guide. New York. 1994.

[19] Taylor D.M. and Williams D.R. Trace element medicine and chelation therapy. Royal Society of Chemistry. Cambridge, UK, 1995.

[20] Cole P.E., Yang S.K. and Crother D.M. Conformational changes of transfer ribonucleic acid. Equilibrium Phase Diagrams. Biochemistry. 11 (23) (1972), 4358-4368.

[21] Dahm S.C. and Uhlenbeck O.C. Role of divalent metal ions in the hammerhead RNA cleavage reaction. Biochemistry. 30 (39) (1991). 9464-9469.

[22] Misra V.K. and Draper D.E. The linkage between magnesium binding and RNA folding. J. Mol. Biol. 317 (2002), 507-521.

[23] Špringer T., Šipová H., Vaisocherová H., Štěpánek J. and Homola J. Shielding effect of monovalent and divalent cations on solid-phase DNA hybridization: surface plasmon resonance biosensor study. NAR. 38 (20) (2010), 7343-7351.

[24] Felsenfeld G., Davies D.R. and Rich A. Formation of three-stranded polynucleotide molecule. J. Am. Chem. Soc. 79 (8) 1957, 2023-2024.

[25] Broitman S.L., Im D.D., Fresco J.R., Formation of the triple-stranded polynucleotide helix, Poly(AAU). Proc. Natl. Acad. Sci. 84 (1987), 5120-5124.

[26] Chalikian T.V., Volker J. Plum G.E. and Breslauer K.J. A more unified picture for the thermodynamics of nucleic acid duplex melting: A characterization by calorimetric and volumetric techniques. Proc. Natl. Acad. Sci. 96 (1999), 7853-7858.

[27] Ross P.D. and Howard F.B. The Thermodynamic contribution of the 5-Methyl group of thymine in the two- and three-stranded complexes formed by Poly(dU) and Poly(dT) with Poly(dA). Biopolymers. 68 (2003), 210-222.

[28] Sorokin V.A., Valeev V.A, Gladchenko G.O. Degtiaar M.V. Karachevtsev V.A. and Blagoi Y.P. Mg^{2+} ion effect on conformational equilibrium of poly A · 2 poly U and poly A poly U in aqueous solutions. International Journal of Biological Macromolecules. 31 (2003), 223-233.

[29] Brahms S. and Brahms J.G. DNA with adenine tracts contains poly(dA)·poly(dT) conformational features in solution. NAR. 18 (6) (1990), 1559-1564. (and citations therein)

[30] Brown P.M. and Fox K.R. DNA triple-helix formation on nucleosome-bound poly(dA)[poly(dT) tracts. Biochem. J. 333 (1998), 259-267. (and citations therein)

[31] Premilat S. and Albiser G. X-ray Fibre Diffraction study of an elevated temperature structure of Poly(dA)·Poly(dT). J. Mol. Biol. 274 (1997), 64-71.

[32] Arzumanov A., Godde F., Moreau S., Toulme J.J., Weeds A. and Gait M.J. Use of the fluorescent nucleoside analogue benzo[g]quinazoline 20-Omethyl- beta-D-ribofuranoside to monitor the binding of the HIV Tat protein or of antisense oligonucleotides to the TAR RNA stem-loop. Helv. Chim. Acta 83 (2000) 1424–1436.

[33] Al-Hashimi H.M., Pitt S.W., Majumdar A., Xu W., Patel D.J. Mg^{2+}-induced variations in the conformation and dynamics of HIV-1 TAR RNA probed using NMR residual dipolar couplings. J. Mol. Biol. 329 (2003), 867–873.

[34] Olejniczak M., Gdaniec Z., Fischer A., Grabarkiewicz T., Bielecki L. and Adamiak R.W. The bulge region of HIV-1 TAR RNA binds metal ions in solution. NAR. 30 (19) (2002), 4241-4249.

[35] Klaver B. and Berkhout B. Evolution of a disrupted TAR RNA hairpin structure in the HIV-1 virus. The EMBO Journal. 13 (11) (1994), 2650-2659.

[36] Cordingley M.G, LaFemina R.L, Callahan P.L., Condra J.H., Sardana V.V., Graham D.J., Nguyen T.M., LeGrow K., Gotlib L., Schlabach A.J. and Colonno R.J. Sequence-specific interaction of Tat protein and Tat peptides with the transactivation-responsive sequence element of human immunodeficiency virus type 1 in vitro. Proc. Natl. Acad. Sci. 87 (1990) 8985-8989.

[37] Berkhout B. and Jeang K.T. Trans activation of human immunodeficiency virus type 1 is sequence specific for both the single-stranded bulge and loop of the trans-acting-responsive hairpin: a quantitative analysis. Journal of Virology. 63(12) (1989), 5501-5504.

[38] Hrabáková J. Investigation of heavy metal ion interaction with important biomolecules. MSc. Diploma Thesis. Charles University in Prague. Prague. 2003.

[39] Kankia B.I. Mg^{2+}-induced triplex formation of an equimolar mixture of poly(rA) and poly(rU). NAR. 31 (17) (2003), 5101-5107.

[40] Kankia B.I. Binding of Mg^{2+} to single-stranded polynucleotides: hydration and optical studies. Biophysical Chemistry 104 (2003), 643–654.

[41] Kankia B.I. Inner-sphere complexes of divalent cations with single-stranded Poly(rA) and Poly(rU). Biopolymers. 74 (2004), 232-239.

[42] Willemsen A.M. and Van Os G.A.J. Interaction of magnesium ions with poly A and poly U. Biopolymers. 10 (6) (1971) 945-960.

[43] Blagoi Y., Gladchenko G., Nafie L.A., Freedman T.B., Sorokin V., Valeev V. abd He Y. Phase Equilibrium in Poly(rA)·Poly(rU) Complexes with Cd^{2+} and Mg^{2+} Ions, studied by ultraviolet, infrared, and vibrational circular dichroism spectroscopy. Biopolymers. 78 (5) (2005), 275-286.

[44] Espinoza Herrera S.J. and Štěpánek J. Raman study of magnesium induced conversion of polyU·polyA duplexes to polyU·polyA·polyU triplexes. Spectroscopy. 24 (3-4) (2010), 445-448.

[45] McGhee J.D. and von Hippel P.H. Theoretical aspects of DNA-protein interactions: co-operative and non-co-operative binding of large ligands to a one-dimensional homogeneous lattice. J.Mol.Biol. 86 (1974), 469-489.

[46] Benevides J.M., Tsuboi M., Bamford J.K.H. and Thomas G.J, Jr. polarized Raman spectroscopy of double-stranded RNA from bacteriophage phi6: local Raman tensors of base and backbone vibrations. Biophys J. 72 (1997), 2748-2762.

[47] Liquier J., Gouyette C., Huynh-Dinh T. and Taillandier. Raman spectroscopy of nucleic acid triple helices. J Raman Spectrosc. 30 (1999), 657-666.

[48] Guan Y. and Thomas G.J., Jr. Vibrational analysis of nucleic acids. III. Conformation-dependent Raman markers of the phosphodiester backbone modeled by dimethyl phosphate. J Mol Struct 379 (1996) 31-41.

[49] Hanuš, J., Štěpánek, J., Turpin P.-Y. and Bok J. Formation and stability of nucleotide complexes: Raman titration investigation. J Mol Struct. 480-481 (1999), 437-442.

[50] Espinoza Herrera S.J., Barvík I. and Štěpánek J. Spectroscopic study of magnesium effect on stability of RNA and DNA triple strand polynucleotide. AIP Conference Proceedings. 1267 (2010), 613-614.

[51] Movileanu L., Benevides J.M., and Thomas G.J., Jr. Temperature dependence of the Raman spectrum of DNA. Part II. Raman Signatures of Premelting and Melting Transitions

of Poly(dA)·Poly(dT) and Comparison with Poly(dA-dT)·Poly(dA-dT)J. Biopolymers. 63 (2002), 181-194.

[52] Thomas G.J., Jr., Benevides J.M., Overman S.A., Ueda T., Ushizawa K. and Tsuboi M. Polarized Raman spectra of oriented fibers of A DNA and B DNA: anisotropic and isotropic local Raman tensors of base and backbone vibrations. Biophys J. 68 (3) (1995), 1073-1088.

[53] Benevides J.M., Overman S.A., Thomas G.J., Jr. Raman, polarized Raman and ultraviolet resonance Raman spectroscopy of nucleic acids and their complexes. J Raman Spectrosc. 36 (2005):279-299

[54] Vachoušek J. and Štěpánek J. Raman study of HIV TAR structural stability. 22 (4) (2008), 267-277.

[55] Ottová P. Mikrokalorimetrické studium termodynamické stability hybridních komplexů nukleových kyselin (thermodynamic stability of hybrid nucleic acid complexes: microcalorimetric study) MSc. Diploma Thesis. Charles University in Prague. Prague. 2009.

[56] Hobro A.J., Rouhi M., Blanch E.W. and Conn G.L. Raman and Raman optical activity (ROA) analysis of RNA structural motifs in Domain I of the EMCV IRES. NAR. 37 (4) (2007), 1169-1177.

[57] Abdelkafi, M., Leulliot, N., Baumruk, V., Bednarova, L., Turpin, P.Y., Namane, A., Gouyette, C., Huynh-Dinh, T., Ghomi, M., Structural features of the UCCG and UGCG tetraloops in very short hairpins as evidenced by optical spectroscopy. Biochemistry 37 (1998), 7878-7884.

[58] Abdelkafi, M., Leulliot, N., Ghomi, M., Herve du Penhoat, C., Namane, A., Gouyette, C., Huynh-Dinh, T., Baumruk, V., Turpin, P. Y., UNCG tetraloops in short oligoribonucleotides reveal high thermodynamic stability and unusual structural properties in aqueous phase as confirmed by optical and NMR spectroscopies. J.Mol.Struct. 408/409 (1997), 241-245.

[59] Baumruk, V., Gouyette, C., Huynh-Dinh, T., Sun, J.-S., Ghomi, M., Comparison between CUUG and UUCG tetraloops: thermodynamic stability and structural features analyzed by UV and vibrational spectroscopy. NAR. 29 (19) (2001), 4089-4096.

[60] Leulliot, N., Baumruk, V., Abdelkafi, M., Turpin, P.Y., Namane, A., Gouyette, C., Huynh- Dinh, T., Ghomi, M., Unusual nucleotide conformations in GNRA and UNCG type tetraloop hairpins: evidence from Raman markers assignments. NAR 27 (5) (1999), 1398-1404.

LIST OF PUBLISHED PAPERS

Shirly Josefina Espinoza Herrera and Josef Stepanek. Raman study of magnesium induced conversion of polyU-polyA duplexes to polyU-polyA-polyU triplexes. Spectroscopy 24 (2010): 445–448. **Supplement 1**

Shirly Josefina Espinoza Herrera, Ivan Barvik, Jr., and Josef Stepanek. Spectroscopic Study of Magnesium Effect on Stability of RNA and DNA Triple Strand Polynucleotides. AIP Conference Proceedings 1267(2010): 613-614. doi:10.1063/1.3482706 **Supplement 2**

Pavla Ottova, Shirly Josefina Espinoza Herrera, Josef Stepanek. Magnesium Effect on Premelting Transitions in Nucleic Acids: DNA Duplex and RNA Hairpin Models. Journal of Molecular Structure (2011) (submitted revised version according to the referees‘ remarks).

Pavla Ottova, Shirly Josefina Espinoza Herrera, Josef Stepanek. Structural stability of apical TAR hairpin and its sensitivity to magnesium ions. Biophysical Journal (submitted)

Shirly Josefina Espinoza Herrera, Ivan Barvik, Jr., and Josef Stepanek. Specific Magnesium Binding to PolyU-PolyA-PolyU triplexes. (manuscript is just completed)

PARTICIPATION IN INTERNATIONAL CONFERENCES. PUBLISHED ABSTRACTS:

Talks:

Espinoza Herrera SJ. and Stepanek J. Specific Magnesium Interaction with RNA Triplexes. RNA Club 2008. November 28, 2008. Prague, Czech Republic; Book of Abstracts, PřF UK 2008 (ISSN 1214-8598), p.4

Posters:

Espinoza Herrera S.J., Vachousek J. and Stepanek J. Magnesium Effect on Formation and Stability of Hybrid Nucleic Acids Complexes. Conference proceedings XII ECSBM. Bobigny, France (2007). p116.

Espinoza Herrera SJ. and Stepanek J. Raman Monitoring of a Specific Magnesium Binding to PolyU-PolyA-PolyU triplexes. Proceedings of XXIst ICORS. Withnall and Chowdhry. London (2008). 906-907.

Espinoza Herrera SJ. and Stepanek J. Raman Characterization of the Specific Magnesium Interaction with RNA Triplexes. Book of Abstracts of ICAVS-5. (2009). 99-100.

Espinoza Herrera SJ., Barvik I., Jr., and Stepanek J. Spectroscopic Study of Magnesium Effect on Stability of RNA and DNA Triple Strand Polynucleotides. Book of Abstracts of XXII ICORS. (2010).

SUPPLEMENTS